



OPEN

Design, development, and preclinical evaluation of pirfenidone-loaded nanostructured lipid carriers for pulmonary delivery

Ananda Kumar Chettupalli¹✉, Anitha Kakkerla², Rajendra Kumar Jadi³, Pavani Uppu⁴, Mohammed Ghazwani⁵✉, Umme Hani⁶, Padmanabha Rao Amarachinta³, Peri Sarvani³ & M. Akiful Haque⁷

Pirfenidone is an antifibrotic and anti-inflammatory drug used for the management of idiopathic pulmonary fibrosis. The current oral delivery of PD has multiple drawbacks, including first-pass metabolism and gastrointestinal discomfort. Efforts have been made to create nanostructured lipid carriers (NLCs) using solid lipids, liquid lipids, and surfactants through an emulsification process followed by ultrasonication to achieve sustained drug release. A central composite design (CCD) utilizing response surface methods (RSMs) was employed to develop and optimize the formulation. The assessed characteristics included particle size distribution, surface topography, drug entrapment efficiency, in vitro drug release, and kinetic profiles in animal models. Cytotoxicity experiments were performed on HepG2 and Caco-2 cell lines and compared with that of PD-NLCs. The optimized formulation yielded a particle size of 159.8 ± 3.46 nm and an encapsulation efficiency of $81.4 \pm 7.1\%$ after 10 freeze-thaw cycles of homogenized lipid carriers. In vitro tests assessing various tested flow rates revealed that over 95% of the released drug was retrieved. In vitro studies showed that the PD-loaded nanostructured lipid carrier (NLC) was more cytotoxic to HepG2 and Caco-2 cells than a pure aqueous solution of the drug. Using 25% w/w sorbitol as a cryoprotectant, the findings showed no variation in the properties of NLC before and after freeze-drying. PD-NLCs carriers were shown to have better bioavailability, longer retention time in the lung, and a 15.94-targeting factor related to the PD aqueous solution. Hence, the outcomes confirmed the potential of the PD-NLCs formulation to improve the efficacy of the drug in inhalation therapy.

Keywords Pirfenidone, Nanostructured lipid carriers, Central composite design, Lung targeting, HepG2, Caco2, Pulmokinetic parameters, Bioavailability

Abbreviations

PD	Pirfenidone
LN	Lipid nanoparticles
SLNs	Solid lipid nanoparticles
O/W	Oil-in-water
NLCs	Nanostructured lipid carrier
RSMs	Response surface methods
HPH	High-pressure homogenization
CCD	Central composite design

¹Department of Pharmaceutical Sciences, School of Medical and Allied Sciences, Galgotias University, Greater Noida, Uttar Pradesh 203201, India. ²Department of Pharmacy, University College of Technology, Osmania University, Hyderabad, Telangana 500 007, India. ³Department of Pharmaceutics, School of Pharmacy, Anurag University, Venkatapur, Ghatkesar, Medchal, Hyderabad, Telangana 500088, India. ⁴Netaji Institute of Pharmaceutical Sciences, Kakatiya University, Somidi, Kazipet, Warangal, Telangana 506009, India. ⁵Department of Pharmaceutics, College of Pharmacy, King Khalid University, 62223 Al Faraa, Abha, Saudi Arabia. ⁶Department of Pharmaceutics, College of Pharmacy, King Khalid University (KKU), 61421 Abha, Saudi Arabia. ⁷School of Pharmacy, Anurag University, Venkatapur Ghatkesar Rd, Hyderabad, Telangana 500088, India. ✉email: anandphd88@gmail.com; myghazwani@kku.edu.sa

ZP	Zeta potential
PDI	Polydispersity index
PS	Particle size
DH	Hydrodynamic diameter
AFM	Atomic force microscopy
FTIRFTIR	Fourier transform infrared spectroscopy
XRD	X-ray diffraction pattern
DSC	Differential scanning calorimeter
PBS	Phosphate-buffered solutions
DMEM	Dulbecco's modified Eagle's medium
FBS	Fetal bovine serum
HBSS	Hanks' balanced salt solution
LY	Lucifer yellow
BP	Blood plasma
AP	Aqueous plasma
IAEC	Institutional Animal Ethics Committee
NIN	National Institute of Nutrition
BAL	Bronchoalveolar lavage
LH	Lung homogenate
BAL	Broncho alveolar lavage

Pirfenidone (PD), also known as 5-methyl-1-phenylpyridin-2-one, aids in the treatment of idiopathic pulmonary fibrosis (IPF) by reducing the progression of fibrotic and inflammatory processes in various tissues. Some of the actions of PD that have been reported to contribute to its anti-fibrotic impact are the modulation of inflammatory cytokines and growth factors, attenuation of fibroblast proliferation, and inhibition of collagen synthesis¹. Clinically, in India, Europe, Japan, and China, PD is the foremost enteral drug (Esbriet[®] or Pirespa[®]) used for treating IPF^{2,3}. However, systemic adverse effects are common when PD is administered orally, including phototoxic skin reactions (responses of the skin to light), digestive discomfort, and liver dysfunction^{4,5}. Notably, after oral administration of PD, the incidence of phototoxic skin responses was over 50% in a clinical experiment. Previous research⁶ partially identified the mechanism of PD-induced phototoxicity, attributing it to the high skin exposure levels of PD.

Nanoparticle formulations have been extensively explored as potential novel drug delivery technologies because of their capacity to increase drug absorption and bioavailability. Among these formulations, lipid nanoparticles (LN) are a promising approach for delivering low-bioavailability medicines. Incorporating active molecules into a solid lipophilic matrix of 150–300 nm (may reach 50–1000 nm) particle size is the hallmark of LN and was first developed by Professor RH Muller^{7,8}. Solid lipid nanoparticles (SLNs), mainly constituted of a solid-lipid matrix, are the first generation of LNs. This LN is developed from oil-in-water (O/W) nano-emulsions, but with solid lipids as an alternative to liquid lipids in the oil droplets. Owing to their many benefits over other organic nanoparticles, they have garnered significant interest. SLNs have excellent *in vivo* stability due to their solid state at physiologic temperature⁹. Additionally, they allow for the gradual release of any drug that has been incorporated into the product, ensuring the highest level of safety. Good tolerability and biodegradability are hallmarks of the excipients used in these formulations.

After the limitations of SLNs were identified, new NLCs were formed. By decreasing the system crystallinity and improving drug encapsulation, NLCs preserved the same benefits as SLNs, while adding additional benefits. It has been reported that the drug escapes from SLNs during storage because the flawless crystalline matrix created following solidification reduces the encapsulation efficiency. NLCs, on the other hand, are not entirely lipid-based; instead, they contain lipid solids and liquids. Incorporating a liquid lipid improves drug entrapment within the nanoparticle core and prevents expulsion during storage^{10,11} due to defects in the lipid crystalline matrix. Coalescence, which is common in traditional emulsions, is avoided because of the solid matrix of NLCs, which improves the stability of the lipid system. One everyday use of these nanoparticles is the oral administration of medicines. They help make drugs that are not very soluble and are more effective when taken orally¹². They may prevent the degradation of active molecules from being degraded in the digestive system.

Moreover, their lipid composition may help target the lymphatic system^{13,14}. The lymphatic system distribution is a promising option for the oral administration of several therapeutic molecules¹⁵. LN facilitate drug absorption and, due to their composition and nano size, can enter the lymphatic system¹⁶. Additionally, enterocytes can absorb chylomicron-induced lipid breakdown products. In this circumstance, the chylomicrons carrying the lipids and medicines and transported from the thoracic duct to the subclavian vein in the neck allow their associated drugs to avoid first-pass metabolism in the liver and remain in circulation for a longer duration. Therefore, several NLC preparations have been shown to improve the oral bioavailability of various drugs. For instance, compared to the drug solution, the oral BA of Nintedanib was increased by a factor of 3.13 when loaded onto NLCs¹⁷. The bioavailability and lymphatic transport of ibrutinib were much higher in brutinib-loaded NLCs than in the free drug¹⁸. NLCs synthesized with the anthelmintic drug mebendazole demonstrated enhanced lymphatic flow and prevented drug metabolism in the first pass effect¹⁹.

Multiple statistical experimental designs have recently been used to optimize formulations with fewer trials and to identify the relative relevance among variables²⁰. Several studies have shown that RSMs are helpful in estimating the connection between independent and dependent factors when interactions among the variables are complex²¹. This includes the optimization of alternative formulations, such as lipid particles. The three components of the experimental design correspond to three levels of CCD located at the center and on the edges of the process space. This cube contained no vertices, making it easy to avoid CCD tests that use extreme factors.

The CCD requires fewer iterations than other three-level response surface design models. To that end, CCD helps optimize a wide range of nanocarriers for several uses²².

This study is novel because it seeks to optimize the technique by which oral PD-loaded NLCs of 200 nm are prepared by high-pressure homogenization (HPH) and ultrasonication. The impact of manufacturing variables on the physicochemical characteristics and stability of NLCs was investigated using repeated measures two-way ANOVA. This study aimed to use a quality-by-design methodology to develop a novel PD-loaded NLCs formulation for oral delivery. The components utilized to prepare the NLCs were selected during the preformulation stage. The impact of components on NLCs' physical properties of NLCs was investigated, and the best formulation was chosen using CCD²². After determining which PD-loaded NLCs achieved the best performance, their zeta potential (ZP), polydispersity index (PDI), particle size (PS), crystalline state, and drug-excipient compatibility were examined.

Furthermore, the stability of the ideal NLCs was studied for six months. Finally, *in vitro* cytotoxicity against HepG2 and Caco-2 lung cell lines was evaluated. *In vitro* release studies were conducted in simulated gastrointestinal fluids to determine how the PD drug release system works. The overview of the present study is depicted in Fig. 1.

Materials and methods

Materials

Biophore India Pharmaceuticals Pvt. Ltd., Hyderabad, Telangana, India, Gifted PD as a gift sample. Glyceryl monostearate (GMS), Compritol 888 ATO, and Precirol ATO-5 were gifts from Gattefosse (Mumbai, India). SD Fine Chemicals Limited Oleic Acid and Tween 20 and 80 (polyoxyethylene sorbitan monooleate) were purchased. The dialysis membrane (molecular weight: 12,000 and 14,000) and Nanosep Centrifugal filters were obtained from Hi-Media and Pall Life Sciences in Mumbai, India (Omega Membrane, MWCO 100 kDa), respectively. All studies used Millipore-Direct Q UV water from Millipore, France. All other compounds and substances used in this study were of analytical grade.

Quantitative analysis by high-performance liquid chromatography (HPLC)

Quantitative studies of PD were conducted using a 1100-HPLC equipped with a Diode Array Detector (Agilent Technologies, Italy) and an Eclipse XDB-C₁₈ column with 3.5 μ m of internal diameter and 150 \times 4.6 mm dimensions²³. All examinations were conducted using an analytical technique with a 0.4 mL/min flow rate and a mobile phase consisting of a 70:30 Acetonitrile/Phosphate Buffer solution (i.e., 1.36 g KH_2PO_4 in 1000 mL Millipore water, pH 3.3, adjusted with triethylamine and ortho-phosphoric acid). The temperature was set to

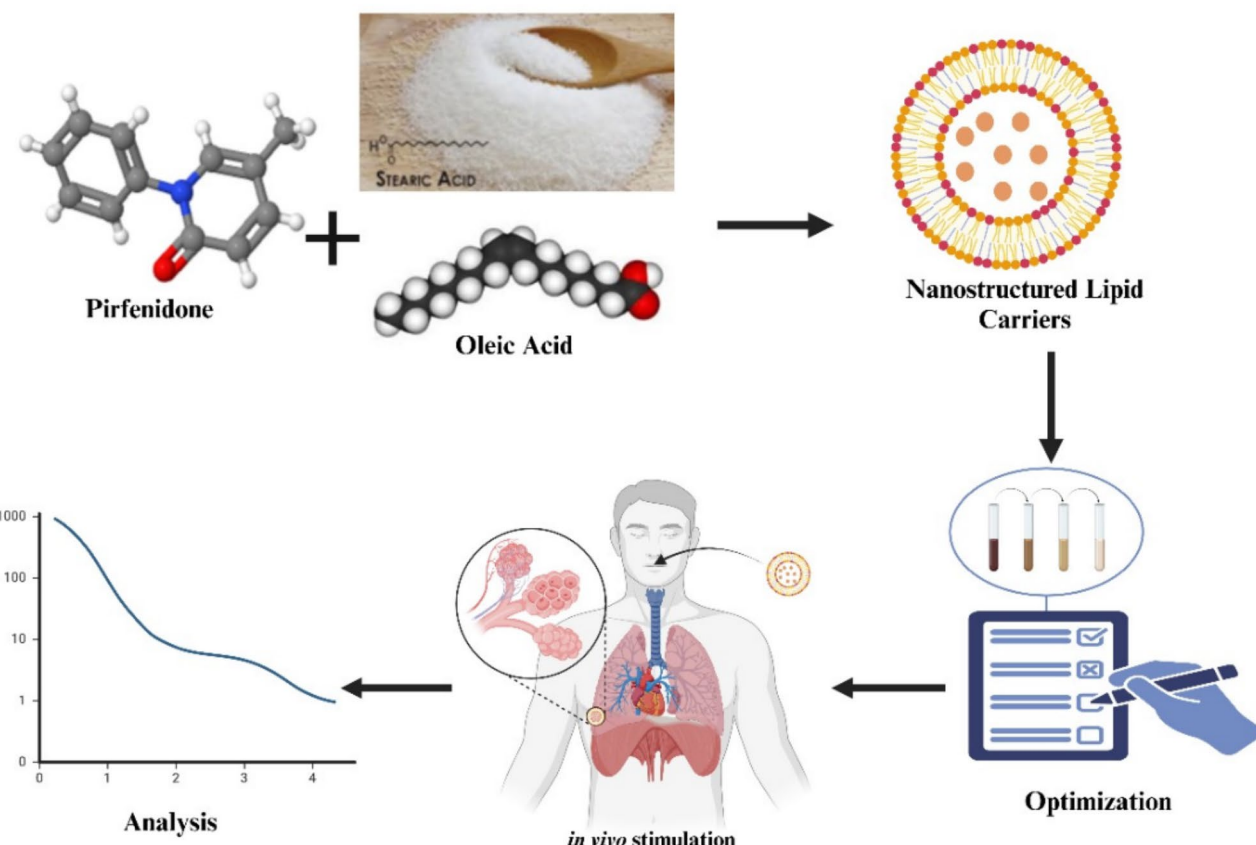


Fig. 1. Overview of present study.

25 °C, and UV-visible spectra were collected between 200 and 600 nm. All the chromatograms were obtained at a wavelength of 312 nm²⁴. A linear association was observed in the concentration range of 10–0.05 µg ($R^2=0.9999$).

Preformulation study

Selection of solid and liquid lipids

We were able to establish solid and liquid lipids with higher solubilizing capabilities by evaluating PD's solubility of PD in various carriers. The formulation of NLCs was guided by the solubility of PD in various oils. Experiments showed that cetyl alcohol, Precirol ATO 5, glyceryl monostearate, Compritol 888 ATO, Stearic acid, Dynasan 114, myristic acid, and Gelucire® 43/01 were all components of the selected solid lipids. All that was done was put 20 mg of PD into a test tube, heat it to 75 °C with magnetic stirring, and then add solid lipid in 200 mg increments. This was performed until the lipid melted entirely and was clear. Glyceryl monostearate is a popular lipid in the cosmetic and drug industries. Monoacylglycerols and diacylglycerols are found in glyceryl monostearates. Chemically, glyceryl palmitostearate (Precirol ATO 5) comprises the fatty acids palmitic acid, stearic acid, and other mono-, di-, and tri-acyl glycerols in the form of Precirol ATO5. When the drug dissolves, glyceryl palmitostearate is released. Compritol 888 ATO contains mono- and triacylglycerols, and diacylglycerols containing behenic acid. Glyceryl palmitostearate and glyceryl dibehenate, both crystalline compounds, have defects in their lattice structures that make entrapment inevitable. Dynasan 114 is a trimyristin composed of plant-based myristic acid and glycerin. Stearic acid, a lipid typically derived from animals and plants, is often used in NLCs. The quantity of lipids used to determine PD's solubility²⁵.

Determination of the optimal ratio of solid to liquid lipid

Mixtures of solid, liquid forms of lipids, with solid-to-liquid lipid ratios ranging from 50:50 to 90:10 (w/w), were kept at 80 °C for 1 h with moderate agitation after being tested for their effects on PD solubility. Visual inspection of phase separation under melted conditions allowed us to evaluate the compatibility of solid lipids and oil. Next, room temperature was chosen for the mixtures. The miscibility of the components was tested by spreading a cooled sample of the mixes onto filter paper and looking for an oil droplet trail²⁵.

Determination of the optimal drug to lipid phase ratio

Empirical research has led to the discovery of the best lipid combination for improving PD solubility. In a nutshell, 80 °C was used to melt 2 g of the lipid phase, created with an ideal solid-to-liquid lipid ratio. The liquid was then magnetically stirred, and 10 mg increments of PD were added. To determine whether PD was no longer solubilized in the lipid phase, the addition of PD was maintained until opalescence or a precipitate formed. We ignored the last percentage and calculated the solubility of PD using the third-to-last portion²⁵.

Selection of surfactant

To determine which surfactants would be most effective in emulsifying NLCs, a comprehensive investigation was conducted in which individual surfactants and mixtures of surfactants were introduced into the molten lipid phase and titrated with double-distilled water. The surfactant was selected repeatedly based on its solubility. A ternary phase diagram was constructed to optimize the surfactant with the highest emulsifying potential after determining drug solubility in surfactants. Surfactants were incorporated into the liquid lipid state at varying concentrations while the mixture was heated and stirred. The results were recorded every time the lipid surfactant mixture was diluted by the addition of²⁶.

Preparation of NLC system

To construct an NLC formulation, the amounts of the components selected in the trials were optimized using a detailed approach²⁷. The emulsification-ultrasonication method produced PD-loaded NLCs^{28,29}. In order to create the aqueous phase, 180 mg of Poloxamer 188 (i.e., 0.9% w/v) was dissolved in 20 mL phosphate buffer solution (PBS). In contrast, the lipid phase composed of stearic acid (i.e., 7% w/v), 3% w/v oleic acid as solid-lipid, and 5% w/v Tween 20 (HLB≈16.7) chosen as the liquid-lipid (HLB required for stearic and oleic acid: 18.6 and 1, respectively). Lipids were combined with 10 mg of PD obtained from an aqueous medium. Two separate but concurrent water and oil solutions were heated to 85±2 °C and magnetically agitated at 250 rpm for 10–30 min to assist in melting and dissolving the components, and homogeneous blending. The water bath was maintained at steady temperature using a thermometric probe. The two hot solutions were combined with an aqueous phase, poured into the oil phase, and then emulsified for 10 min at 5000 rpm in a T25 Ultra-Turrax³⁰. The resulting microemulsion was optimized using an ultrasonic homogenizer and a Sonopus HD 2200 fitted with a KE-76 probe. The Ultrasonication was performed at 10% power for half a second on and off. The sample was subjected to two-minute cycles at 25±2 °C (room temperature), followed by one-minute cycles in a water bath maintained at 20±2 °C. The size and ZP of the NLC formulation measured by the dynamic light scattering (DLS) technique with computerized equipment (Malvern Zetasizer, UK) and analyzed using “DTS nano” software (The latest version available for this software is v1.51, url: <https://www.malvernpanalytical.com/en/support/product-support/dts-software-update-v1-51>). The entrapment efficiency (EE) was determined using ultra-centrifugal filtering devices.

CCD for optimization of NLC system

Preliminary screening experiments were used to determine the vital characteristics that might impact the desired and optimal qualities of the NLCs system for oral distribution. According to the results of these primary studies, the total lipid content, surfactant concentration, and sonication duration may significantly impact the quality of the NLCs used in oral delivery³¹. Constraints were established to limit the effects of any observable variables on the properties of the formulation^{32,33}. The independent and dependent factors utilized in the CCD design

Parameter	Low (-1)	Medium (0)	High (+1)
Independent variables			
X1 (% w/v)	6	8	10
X2 (% w/v)	0.5	0.75	1.5
X3 (min)	10	20	30
Dependent variables			
Y1 (nm)	159.8±3.46	520.6±11.29	
Y2 (%)	40.5±3.1	81.4±7.1	
Zeta potential	-11.6±0.26	-32.5±0.64	
Drug Loading	6.59±0.9	15.62±0.9	
PDI	0.13±0.03	0.42±0.61	

Table 1. CCD was used to optimize the PD-NLCs.

Run	X1 (%w/v)	X2 (%w/v)	X3 (min)	Y1 (nm)	Y2 (%)	Zeta potential (mV)	DL (%)	PDI
1	0	-1.681	0	370.2±7.64	56.8±9.7	-11.6±0.26	9.64±0.6	0.23±0.01
2	0	0	-1.68	295.4±3.49	65.3±8.3	-28.3±0.13	10.21±0.9	0.34±0.23
3	0	0	0	329.2±4.15	60.3±9.2	-20.9±0.56	12.59±0.1	0.21±0.01
4	-1	-1	1	330.6±3.12	60.4±3.5	-18.3±0.11	10.35±0.8	0.34±0.02
5	-1	-1	-1	461.5±10.23	47.8±6.4	-22.4±0.37	11.38±0.1	0.19±0.23
6	1.681	0	0	520.6±11.29	40.5±3.1	-20.7±0.28	8.64±0.2	0.29±0.21
7	0	0	0	325.9±8.43	64.1±8.2	-26.1±0.34	9.21±0.5	0.41±0.11
8	-1.68	0	0	345.7±3.26	57.9±6.5	-26.1±0.28	10.46±0.6	0.33±0.31
9	0	0	0	394.5±1.89	49.1±6.2	-26.2±0.22	8.64±0.2	0.29±0.21
10	1	1	1	159.8±3.46	81.4±7.1	-32.5±0.64	15.62±0.9	0.13±0.03
11	-1	1	-1	330.7±7.25	61.7±6.2	-14.3±0.16	13.69±0.3	0.18±0.53
12	0	1.681	0	285.3±6.18	65.2±1.2	-20.5±0.52	10.52±0.4	0.37±0.21
13	-1	1	1	394.9±12.46	52.6±3.5	-18.2±0.34	6.89±0.7	0.33±0.13
14	0	0	0	330.6±9.14	61.6±2.9	-23.8±0.61	8.43±0.9	0.28±0.02
15	1	-1	1	331.7±9.15	61.9±3.9	-26.1±0.08	6.94±0.5	0.29±0.05
16	1	1	-1	387.7±5.24	59.9±4.9	-16.2±0.91	11.52±0.3	0.43±0.13
17	0	0	0	431.9±8.46	42.5±5.3	-18.3±0.68	10.86±0.8	0.39±0.26
18	0	0	0	329.9±1.64	60.4±8.1	-22.4±0.35	9.47±0.6	0.38±0.53
19	1	-1	-1	372.5±5.62	49.3±2.1	-26.3±0.06	6.59±0.9	0.42±0.61
20	0	0	1.681	218.2±3.19	75.9±0.9	-26.3±0.31	11.38±0.2	0.38±0.8

Table 2. Composition of the formulations and the findings employed in the optimization process.

for creating the PD-loaded NLCs are listed in Table 1. Utilizing Design-Expert[®] Version 12.0.3.0 (Stat-Ease Inc., Minneapolis, MN, USA, url: <https://www.statease.com/software/design-expert/>), which had a 3-factor, 3-level CCD design, optimization of NLCs was carried out. The total lipid content (X1), surfactant concentration (X2), and sonication time were the independent variables (X3). The outcomes of the exploratory study that determined high and low values (1, 0, -1) for each independent component are summarized in Table 1. As listed in Table 2, the design included 20 separate experiments, each of which was solved using the following computer-generated quadratic Eq. (1):

$$Y = b_0 + b_1X_1 + b_2X_2 + b_3X_3 + b_{12}X_1X_2 + b_{13}X_1X_3 + b_{23}X_2X_3 + b_{11}X_2^2 + b_{22}X_2^2 + b_{33}X_3^2 \quad (1)$$

Where 'Y' is an observed response for each level combination of the three factors, 'b0' is a constant, 'b1, b2, and b3' are linear coefficients, 'b12, b13, and b23' are interaction coefficients between the three factors, 'b11, b22, and b33' are quadratic coefficients of the observed experimental values, and 'X1, X2, and X3' are values of the three independent variables^{34,35}. The results of the CCD design for improving the formulation of the PD-loaded NLCs are shown in Table 2.

Several statistical metrics were examined to choose the best model, including the 'p-value' adjusted and expected squared correlation coefficients (R^2), and predicted residual sum of squares (PRESS). Once the optimal NLCs formulation has been determined, the desirability function is applied to maximize both the independent variables.

Characterization of NLC dispersions

Particle size, polydispersity index, and ZP

Using a Zetasizer Nano ZS Zen 3600 (Malvern[®] Instruments, UK) at 25 °C and 173° backscatter detection in disposable folded capillary clear cells, ZP, PS, and PDI of the produced PD-loaded NLCs formulations were evaluated. Particle size data were measured using a helium-neon laser and analyzed using a volumetric measure. The PS and PDI were measured after diluting 10 µL of the sample to 1000 µL with deionized water. DLS provides PDI as a measure of the breadth of the particle size distribution and the hydrodynamic diameter (DH) of nanoparticles, which is the intensity-weighted mean diameter of the bulk population. Each number is the mean of at least ten measurements taken during three separate runs of the instrument. No readings were obtained at a temperatures lower than 25 °C³⁶.

Efficacy of encapsulation and drug loading

To assess the Drug Loading (DL) and Drug Entrapment (EE) of the NLCs formulation, we measured the amount of unentrapped drug using Amicon ultra centrifugal filter units (Sigma-Aldrich Ultra-15, MWCO 10 KDa). It was then quantified using HPLC (Waters Corporation, Milford, MA, USA). Waters Instruments Model 1525 pump, Waters Instruments Model 717 Plus auto-injector, and Waters Instruments Model 2487 variable wavelength UV detector were all part of the chromatographic apparatus, along with Millennium PC running software version³⁷.

Unloaded drug particles were dissolved by mixing 1 mL of the NLCs formulation with 2 mL of the diluent. The sample was diluted and placed in an ultra-centrifuge at 8000 rpm for 20 min. The free drug in the aqueous phase infuses into the bottom chamber, whereas the drug entrapped in the nanoparticles is retained in the top portion of the centrifuge tube. The flow-through rate in the bottom chamber was calculated using high-performance liquid chromatography with an autosampler connected to a dual-wavelength absorbance detector. A 125 mm × 4 mm LiChrospher[®] 100 RP-18 and RP-18 column (Merck) was used to measure PD concentration (Kenilworth, NJ, USA). Acetonitrile and double-distilled water (at a 1:1 ratio) were used throughout the mobile phase, and the mixture was eluted isocratically. Samples were dissolved in acetonitrile and fed into a 20 µL sample loop. The efficiency with which the medicine was integrated was measured by calculating the amount of added drug still present in the filtered NLCs after the process. The retention time for the PD-loaded NLCs formulation was 4.56 min, and the flow rate was constant at 0.5 mL/min. In order to determine the NLCs' stability over time, we lyophilized them and stored them at 4 °C. The DL and EE were calculated using the following Eqs. (2 and 3):

$$\% \text{ Entrapment Efficiency (EE)} = \frac{\text{Amount of Drug in NLCs}}{\text{Total amount of drug added}} \times 100 \quad (2)$$

$$\text{Drug Loading (DL)} = \frac{\text{Amount of Drug entrapped}}{\text{Total amount of Lipid} + \text{Total amount of drug in NLCs}} \times 100 \quad (3)$$

Determination of % yield

The nanoparticle weight for each NLCs combination run was added to the initial dry weight of the drug and polymer to determine the percentage yield³⁸. The % yield was determined using Eq. 4 as given below:

$$\% \text{ Yield} = \frac{\text{Weight of Nanoparticles}}{\text{Weight of Drug} + \text{weight of Polymers}} \times 100 \quad (4)$$

Morphological characterization

These methods establish the size, dispersion, and form of the nanoparticles according to²⁶.

Transmission electron microscopy (TEM)

TEM using an Olympus Mega view G2 camera and an accelerating voltage of 80 keV was used to analyze the morphology of PD-loaded NLCs³⁹. These studies included placing a nanoparticle dispersion of optimized PD-loaded NLCs in ultrapure water at the starting concentration on a copper grid coated with a carbon sheet. Subsequently, the thin film was dyed with a phosphotungstic acid solution of 1% weight-per-volume and diluted in distilled water by blotting the excess material off the grid using filter paper. Three minutes after the samples were stained, they were analyzed.

Scanning electron microscopy (SEM)

A Graz Austria ZEISS Ultra 55 scanning electron microscope was used for SEM imaging (Carl Zeiss SMT GmbH, Germany) at the Institute for Electron Microscopy in Graz, Austria. The experiment was carried out by diluting the samples with MilliQ water, placing them on an amorphous carbon grid, leaving them air-dried at room temperature, and finally coating them with chromium⁴⁰.

Atomic force microscopy (AFM)

AFM was used to visualize the morphology of NLCs. Specifically, a Veeco NanoScope Dimension V AFM (Plainview, New York, USA) was utilized along with an RT ESP Veeco tube scanner. We used a low-resonance frequency pyramidal silicon cantilever that resonated at 250–331 kHz. The constant force applied to the cantilever ranged from 20 to 80 N/m, and the scanning rate was 0.5 Hz. The mica was submerged in a solution containing lipid nanoparticles, and then allowed to absorb the particles before any observations were taken. The surfaces were then washed twice with water and allowed to dry naturally⁴¹.

Solid-state characterization

To characterize the dispersion of the Optimized PD-Loaded NLCs in the solid state, Labconco-Freezone 25 was used. Differential scanning calorimetry (DSC), Powder X-ray Diffraction Pattern (XRD), and Fourier transform infrared spectroscopy (FTIR) were used to analyze the solids content after the improved procedure (FTIR).

DSC

DSC thermograms were recorded (CDR-4P, Shanghai, China). Ten milligrams of material were placed in an aluminum dish and subjected to DSC measurements at a heating rate of 10 °C/min and a temperature range of zero four 400 °C. The temperature and energy scales of the DSC instrument were calibrated using magnesium as the standard reference material. A thermal study⁴² was performed on the formulation of a pure drug, stearic acid, oleic acid, poloxamer 188, and optimized PD-loaded NLCs.

FT-IR

The infrared spectra of the pure drug, stearic acid, oleic acid, and the optimized NCs formulation were measured at a resolution of 4 cm⁻¹ using a spectrometer (Bruker EQUINOX 55, Germany) with a wavelength range of 4000–400 cm⁻¹ and covering the whole spectrum. An FTIR spectrometer was used to analyze the IR spectra of nanoparticles and pure components. At the same time, the temperature was held constant at room temperature. Detection of potential interactions that may occur during nanoparticle synthesis. This method involves compressing a thin pellet made of pure drug, stearic acid, oleic acid, and an optimal NCs formulation with KBr. The data were collected between 4000–400 cm⁻¹¹⁷.

Characterization by XRD

The physical properties of the simulations were determined by analyzing the X-ray diffraction patterns produced by the models. Pure drug, stearic acid, oleic acid, poloxamer 188, and the optimized PD-loaded NLCs formulation were employed in sample studies. A D8ADVANC (Bruker, Germany) Powder X-ray diffractometer was used to obtain XRD patterns. We scanned the samples at a rate of 0.02 °/s over a range of 2θ that extended from 3 ° to 40 °⁴³.

In vitro release studies of PD-loaded NLCs

At 37±0.5 °C and 100 rpm, Franz diffusion cells (Logan Instruments, USA) were used to examine the in vitro release of the NLC formulations. Optimization was performed on PD-loaded NLCs before discharge (Table 1). Furthermore, the PD-loaded NLCs formulations were compared to the in vitro release of a pure drug solution in water containing 10 mg of PD (1 mL). To conduct release studies, a semipermeable membrane with a molecular cut-off of 14,000 Da was used. To maintain the sink state and manipulate the acceptor phase, a 3:7 (v/v) mixture of ethanol and PBS (pH 7.4) phosphate-buffered solutions (PBS) was used. The Optimized PD-loaded NLCs (equivalent to 10 mg PD) were placed in the donor chamber and covered with parafilm to prevent dehydration. Two-milliliters samples were taken every half an hour for the next four hours, and so on for the next 12, 20, and forty-eight hours (0.5, 1, 2, 4, 6, 8, 12, 16, 20, 24, and 48 h); the volume of each sample was replaced with a new buffer. HPLC was used to determine the amount of PD in the acceptor medium. The experiments were repeated thrice to ensure accuracy. The proportion of free drugs was calculated and plotted against time. To make sense of the data, many kinetic models have been used, including the zero-order, first-order, second-order, and Higuchi models. The R² correlation coefficient for each case was calculated⁴⁴.

Cell culture

An in vitro study of a Caco-2 colorectal adenocarcinoma line was performed at Aakaar Biotechnologies Private Limited, ankipuram Extension, Lucknow, Uttar Pradesh 226,031, India. The cell lines were purchased from National Centre for Cell Science, Pune, India. Cells of the Caco-2 colorectal adenocarcinoma line were grown in Dulbecco's modified Eagle's medium (DMEM; Thermo Fisher Scientific, India) supplemented with 20% fetal bovine serum (FBS), 100 U/mL penicillin-streptomycin, and 1% L-glutamine, Rod After 80% confluence was reached, cells were trypsinized weekly at a split ratio of 1:3⁴⁵.

MTS assay

As detailed earlier, 5×10³ cells/well Caco-2 cells were seeded per well in 96-well cell culture plates and allowed to mature for 24 h. Then, over the following two hours, cells were exposed to the drug solution and PD-laden NLCs (loaded with drug) at various dilutions. MTS test was performed as previously⁴⁶. Cell viability was calculated as a percentage of the results obtained from the treated and untreated cells (controls).

Permeability study on Caco-2 cells

Cells were seeded at a density of 2×10⁵ cells/well onto 12-well PET transwell plates (1.13 cm² growth surface area and 0.4 m pore size, Greiner Bio-One, Milan, Italy) for permeability investigations. For the first and next weeks, culture medium (DMEM) was introduced to the apical (AP) (0.5 mL) and basolateral (1.5 mL) sides and replenished every three days. The cells were allowed to differentiate for 18–21 days. The integrity of the cellular barrier was assessed using the Lucifer Yellow (LY) permeability test, as previously described⁴⁶. Briefly, Hanks' balanced salt solution (HBSS) for transfer was replaced with DMEM before the transport investigation, and 25 mM HEPES (4-(2-hydroxyethyl)-1-piperazineethanesulfonic acid) was added (pH 7.4). After pre-incubating the Caco-2 cells for two h in GIF and a further two h in simulated intestinal fluid (SIF), the cell monolayer stabilized at 37 °C about 30 min before being exposed to PD-loaded NLCs or a PBS solution of free PD at a final dilution of 1:150 for 2 h. At the end of the experiment, cellular lysates, blood plasma (BP), and aqueous plasma (AP) were

collected for HPLC-DAD analysis⁴⁷. Equation 5 was used to compute the apparent permeability (Papp, cm/s), as follows:

$$P_{app} = \frac{VA}{(AXCD) \left(\frac{\Delta CA}{\Delta t} \right)} \quad (5)$$

Where VA is the volume (mL) of the acceptor (i.e., basal) compartment, A is the surface area (cm²), CD 0 is the concentration (in mM) in the donor (i.e., apical) chamber at the beginning of the experiment, and $\Delta CA / \Delta t$ is the rate (in seconds) at which the concentration of the drug changes in the acceptor (basal) compartment over time (s).

In vitro cytotoxicity studies

PD-loaded NLCs were tested for cytotoxicity against HepG2 cells using a standard CCK-8 assay. HepG2 cells were seeded at a density of 1×10^{-4} on 96-well culture plates. After removing the culture media, the cells were cultured at 37 °C for 24 h with 200µL of different doses of pure drug solution, optimal PD-loaded NLCs, the combination of drug and stearic acid, and negative control (200µL of fetal bovine serum-free culture medium). The cells were stained for 2 h with 10µL of CCK-8. The absorbance was measured at 450 nm using a microplate reader. The findings are presented as a percentage of the absorbance of the negative control. The half-maximal inhibitory concentration (IC₅₀) of the samples was determined.

In-vivo pulmokinetic study

Animals

The Institutional Animal Ethics Committee (IAEC) of Andhra University in Visakhapatnam approved the protocol with reference number: IAEC No: I/IAEC/AU/013/2021WR. The in vivo procedure was performed as per the guidelines of Committee for the Purpose of Control and Supervision of Experiments on Animals (CPCSEA)⁴⁸. Approximately a week before the studies were performed, male Wistar rats were obtained from the National Institute of Nutrition (NIN), Hyderabad. During all times of the experimental, the animals were kept in groups of three in plastic cages with constant environmental controls for temperature (24 ± 1 °C), humidity (5 ± 10%), and light/dark cycles of 12 h light/dark cycles. The rats were provided unrestricted access to water and a standard pelletized chow diet (Mahaveer Enterprises, Hyderabad) *ad libitum*; however, they were required to fast for 18 h prior to the start of the study. The well-being of the animals was assessed regularly during the acclimation period. All in vivo studies complied with the ARRIVE criteria. This study was conducted in accordance with ARRIVE guidelines⁴⁹.

Dosing protocol

Based on earlier findings⁵⁰, a pharmacokinetic investigation was performed using a pure PD solution and PD-loaded NLCs. In brief, urethane solution (1.2 g/kg) was injected intraperitoneally into groups of six albino rats (200–240 g, 12–16 weeks) at random. A 5–7 cm segment of PE200 tubing was cannulated at the tracheal bifurcation after a small midline incision between the fifth and sixth tracheal rings with a 22-gauge needle. Cannula administration of PD-aqueous solution and PD-loaded NLCs (dosage corresponding to 50 µg/kg, body weight) diluted in phosphate buffer saline PBS (pH 7.4) was used in this study⁵¹. After obtaining a bronchoalveolar lavage (BAL) of approximately 8 mL from each rat by aspirating 12 mL of filtered PBS (pH 7.4) pre-warmed to 37 °C, the animals were sacrificed by cervical dislocation at 0.5, 1, 2, 4, 8, and 24 h. Before being analyzed by HPLC for the released and unreleased drug from PD-loaded NLCs, isolated lung and BAL samples were kept at 70 °C.

Lung homogenate (LH) and broncho alveolar lavage (BAL) sample preparation

LH and BAL samples were produced using a liquid-liquid extraction approach. 100 µL of the BAL samples were tainted by the addition of 300µL of an internal standard solution containing 15 µg/mL in methanol for the LH samples and 6 µg/mL for the BAL samples. Extraction was performed using methanol to create an IS standard solution. samples were centrifuged at 7000 rpm for 15 min at 4 °C (AllegraTM 64R Centrifuge, Maharashtra) after being vortexed for 10 min. For quantification, 20µL of the recovered supernatant was fed into an HPLC system. Lung deposition investigations were performed using the same procedures as plasma sample processing, including weighing and homogenizing the lungs with 500µL PBS (pH 7.4).

HPLC analysis of PD content in biological samples

The Developed HPLC method, which was previously published with a modification⁵² was used to assess the amount of PD in the LH and BAL samples obtained, and the findings were verified. This method has been previously published. In the stationary phase, we used a Thermo Scientific ODS Hypersil C-18 column 250 mm in diameter and 4.6 mm in depth. Separation was carried out with the assistance of an HPLC system manufactured in Japan by Jasco (Jasco Intelligent Pump, 2080 Plus, Japan). The flow rate was 1 mL/min, and the mobile phase was made up of methanol, an ammonium acetate buffer with a concentration of 20 millimoles, and 0.2% formic acid in a combination. The flow rate was 1 mL per minute. Using a UV/VIS (Jasco UV 2075, Japan) detector, we determined that the 313 nm wavelength had a retention period of 5.29 ± 0.035 min. The HPLC technique was validated following the standards set out in the ICH Q2(R1) (2005) document to ascertain whether the developed analytical method was practical. The developed technique had a relative standard deviation of %, which is evidence of its accuracy, precision, and stability.

Pharmacokinetic and statistical analysis

The researchers used a non-compartmental approach to determine C_{\max} , T_{\max} , AUC, and CL values for PD in the lungs and BAL fluid (Win Non-Lin Version 5.2.1, NC, USA). Data are presented as mean \pm standard deviation. The pharmacokinetic parameters were subjected to statistical analysis, with results shown as one-way p-values using Student's t-test for independent samples. The significance threshold was set at $P < 0.05$. GraphPad Prism 5.0 was used to conduct all statistical tests (Graph pad software [CA, USA]).

Stability studies in Gastro-Intestinal simulated fluids

The long-term stability of PD-loaded NLCs was evaluated by measuring the retention of PD concentration (R%), nanoparticle size, and PD index (PDI) in simulated gastric fluid (SGF) and SIF⁴⁶. The ingredients for SGF were pepsin (3.2 g), NaCl (2.0 g), and HCl (7 mL), all of which were dissolved in 1 L of water (pH adjusted to 2.0, using 1 M NaOH). An aliquot of PD-loaded NLCs (100 μ L) was diluted in 900 μ L of SGF (dilution factor 1:10) in a PST-60 H-4 Plate Thermo-Shaker for 2 h at 37 °C with continuous shaking at 300 revolutions per minute (Biosan, Riga, Latvia). Materials were digested in SGF, then diluted 1:15 in SIF (pH 7.0) with 0.4 mg/mL lipase, 0.15 mg/mL bile salts, 0.5 mg/mL pan-creatin, and 750 mM CaCl₂, and finally diluted 1:15 in SGF. Afterwards, 4 h were incubated at 37 °C with magnetic stirring at 300 revolutions per minute. Samples were diluted 1:15 in ultrapure water for size and PDI measurements, and 1:10 in EtOH for R% determination after 2–4 h of incubation, as described above. To simulate the dilution that occurs in cell permeation experiments and in vivo after oral administration, PD-loaded NLCs were diluted to a final concentration of 1:150 in SGF and SIF.

Statistical analysis

The p-value of 0.05 in an ANOVA serves as a minimally significant level of difference (V6 graph PAD Prism, CA).

Results and discussion

Preformulation study

To ensure optimal drug encapsulation in nanoparticles, pre-formulation research was conducted to provide the rationale for formulating NLCs, including solid lipid and liquid lipid excipients. Figure 2 shows the outcomes of our investigation on PD solubility in solid and liquid lipids. Solubility (in milligrams per milligram of solid lipid) was the best for stearic acid compared to other lipids. This led to the choice of stearic acid as the final product's solid lipid. The lipid liquid was selected after reviewing the results of previous studies. Oleic acid has been found to produce highly soluble PD⁵³. Oleic acid was settled upon as the preferred lipid liquid.

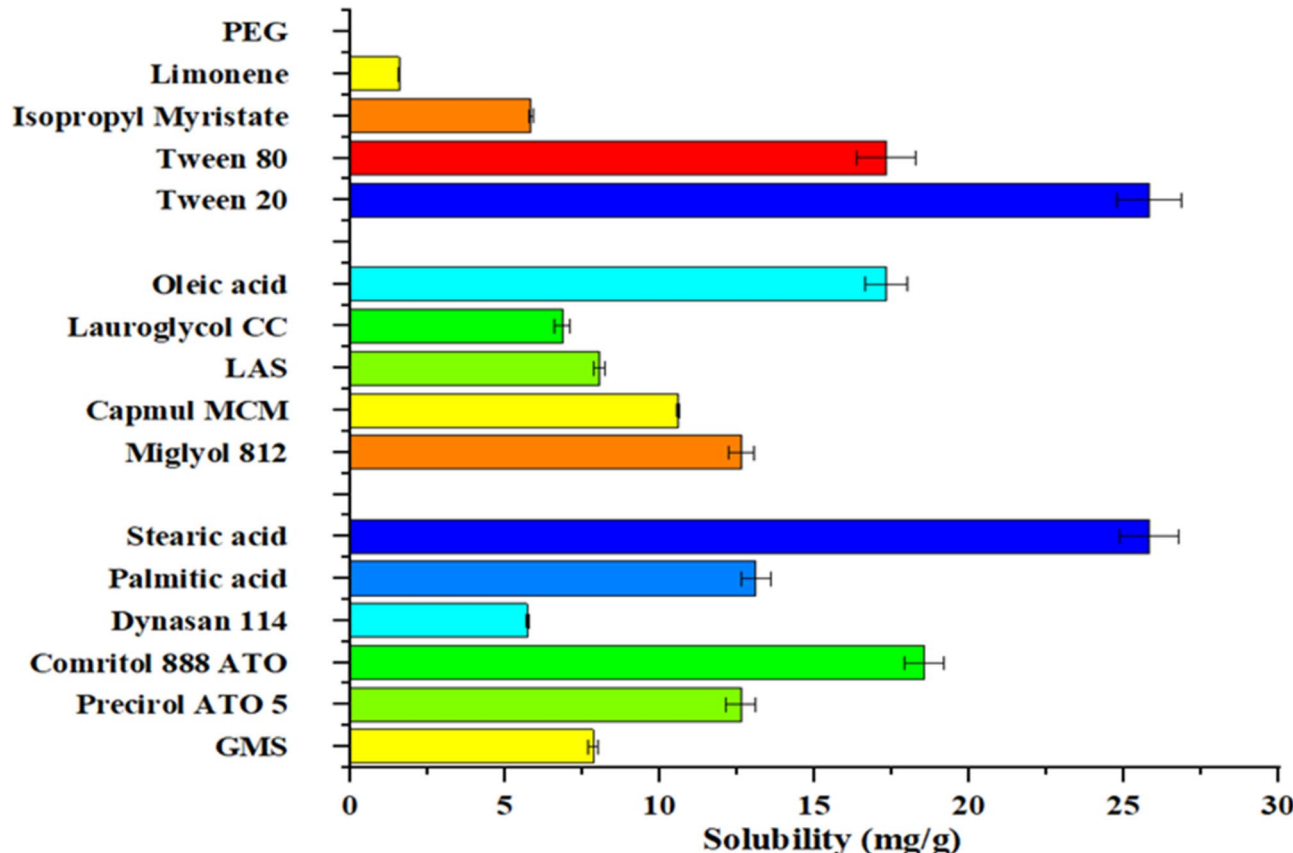


Fig. 2. Solubility determination of PD in various solid lipids, liquid lipids and surfactants.

Mixed solutions of the two lipids were also created with varying lipid-to-oil ratios and agitated at a temperature of 10 °C above the melting point of stearic acid to establish the optimal combination. When melted, both lipids were fully miscible and there was no sign of phase separation in the mixtures. After the mixes had cooled, they were analyzed to ensure that the liquid lipid was completely encapsulated. A filter paper was used to spread the concoctions. Oil was absorbed by the filter paper in overabundance when the ratio of stearic acid to oleic acid (w/w) was 50:50 or 60:40. There was no indication of oil droplets on the filter paper in the 70:30 to 90:10 (w/w) range. To this end, we selected the mixture with the highest liquid lipid concentration; however, there was no discernible oil residue on the filter paper. Therefore, PD-loaded NLCs were formulated at a ratio of 70:30 (w/w).

The chosen lipid combination was evaluated for PD solubility. At 10 °C, above the acid's melting point, the lipid mixture was heated, and PD was added to fractions while being agitated. The lipid content of the mixture was examined to visually evaluate the solubilities of the added fractions. After one hour of vigorous shaking, the maximum solubility of the drug was observed in the form of a persistent precipitate. The quantity of wholly dissolved medicine was used to calculate the solubility rather than the added final portion. The solubility of PD in the lipid mixture was determined to be 36.502.18 mg/g. Because this number is greater than the solubility of stearic acid alone, the inclusion of oleic acid in the lipid mixture improved drug solubility and permitted the encapsulation of a greater quantity of PD. One of the deciding parameters in the formulation was the proportion of medicines used during the first load. As the solubility of the drug in melted lipids decreases with cooling and solidification, the drug may be expelled if the initial loading % is too high⁷. To guarantee that all the drugs would be dissolved in the lipid phase, 3% (w/w) of the lipid mixture was established as the initial loading proportion of PD in NLCs.

Surfactants and co-surfactants stabilize the formulation and facilitate drug solubilization in the lipids. Tween 20 at a concentration of 4.5% was chosen as a surfactant, and Poloxamer 188 was chosen as a co-surfactant, based on the re-dispersibility, phase separation, and hand-in-hand with caking stability of formulations made with different surfactants^{54,55}.

Preparation of PD-Loaded NLCs

HPH, followed by ultrasonication, was used to create PD-loaded NLCs (PD-NLCs). The NLCs were prepared by testing a variety of surfactants (Tween 20, isopropyl myristate, Limonene, and PEG, at concentrations of 0.5 to 1.5%) and lipids (stearic acid and oleic acid at concentrations of 6 to 10%). Although none of the studied combinations produced NLCs, gelation, lump growth, aggregation, and persistent foam were observed. The combination of total lipid (0.6%), Tween 20 (0.5% w/v), sonication period (30 min), and PD was the only formulation that could generate NLCs (10 mg).

In particular, the addition of poloxamer helped the PD and lipid phase merge better, whereas the addition of Tween 20 provided the best HLB for stabilizing the formulation through steric effects. Oleic acid was blended into the mixture to make the medicine more soluble and increase its nutritional value. It is found in almost all lipids, and has the widest distribution of natural fatty acids. Olive fruit contains oleic acid, which is the primary fatty acid in olive oil (*Olea europaea*). 55–80% of olive oil, 15–20% of grape seed oil, and sea buckthorn oil contain oleic acids⁵⁶. Commercial oil, as a dietary supplement, was extracted from oleic acid using cold pressure without solvents and subsequent mechanical filtering. To prepare the nanoparticles, oleic acid was heated to a temperature below its breakdown point of 360 °C. At this temperature, the production of hydroperoxides corresponded with the loss of polyunsaturated fatty acids (PUFA and MUFA, respectively) and saturated fatty acids (SFA). Vegetable oils retain their nutraceutical qualities after encapsulation into NLCs.

CCD: statistical analysis

To obtain the best results for the formation of PD-loaded NLCs, a CCD experimental design was used. Optimized NLCs were produced using a 3-factor, 3-level rotatable CCD. The time spent sonicating (X3), percentage of surfactant (X2), and overall percentage of lipids (X1) were all identified as experimental factors. Table 1 summarizes the results of the exploratory research that determined low and high values (-1, 0, +1) for each independent component. According to the protocol mentioned above, 20 separate tests were performed using experimental design software Design-Expert[®] Version 12.0.3.0 (Stat-Ease Inc., Minneapolis, MN, USA, url: <https://www.statease.com/software/design-expert/>). Table 2 displays the experimental matrices and dependent variable findings for all tests conducted.

An analysis of the findings over various parameters identified the best-fitting model for each answer. A significant p-value with the maximum R² value, rather than a significant p-value signifying a lack of fit, indicated that the mathematical model was a good match. An appropriate signal-to-noise ratio exists because the discrepancy between the anticipated and adjusted R² values is less than 0.2. Each regression coefficient in the model was tested for significance using ANOVA.

The coefficients of variables with < 0.05 significant p-value were the only ones used in the generated polynomial equations. The fact that the answers for PS (Y1) and EE (Y2) both fit into a quadratic model (R² values of 0.9446 and 0.9434, respectively) indicates that there is a significant link between the independent and dependent variables. The model results that matched the best data are reported below, along with the polynomial equations representing each response. Using three-dimensional response surface plots, we determined the influence of each independent variable on the outcome of the responses (Fig. 3, Table 3).

Effect of independent variables on particle size

The sizes of the particles measured were 159.8 ± 3.46 and 520.6 ± 11.29 nm. Based on these findings, the following mathematical equation was derived: Particle size was significantly affected by both independent factors, as determined by ANOVA (Table 4). As shown in the 3D plots of the particle size response, the size of the particles increased as the lipid content decreased and the surfactant concentration increased (Fig. 3). When factor X1 has

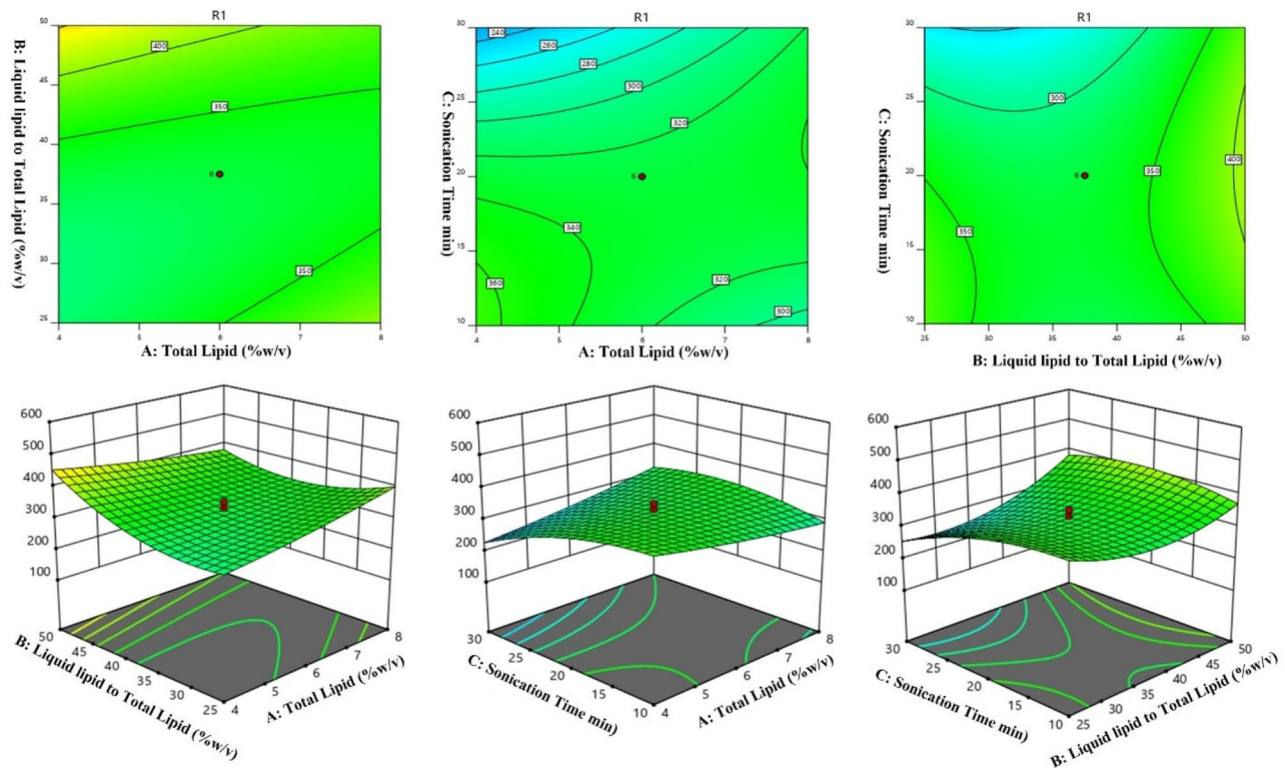


Fig. 3. counter and 3D-response surface plot showing the effect of independent variables on particle size.

Parameter	Source	DF	Sum squares	Mean squares	F value	P-value
SIZE (nm)	Model	9	1.147E+05	12742.41	39.06	< 0.0001
	Residual	10	3262.02	326.20		
	Lack of fit	5	3259.18	651.84	1150.30	< 0.0001
	Pure error	5	2.83	0.57		
% EE	Model	9	1842.65	204.74	38.96	< 0.0001
	Residual	10	52.55	5.25		
	Lack of fit	5	51.05	10.21	34.03	0.0007
	Pure error	5	1.50	0.30		

Table 3. Analyze all models for reaction particle size (Y1) and %EE (Y2).

a positive value, as in (4.6341), the total lipid content has a favorable impact on particle size³¹. These findings do not agree well with those of other studies. Increases in lipid concentration cause the preparation to become more viscous, which in turn causes more particle collisions and aggregation, leading to a bigger particle size^{57,58}. However, opposite results, in which decreasing particle size was observed when the lipid concentration was increased, have been reported by specific investigations. Although the exact reason for this phenomenon is unclear, Vitorino et al.⁵⁹ postulated that it could be related to a lack of dispersion when the lipid phase has a relatively low overall concentration. Alternatively, the positive result (1.8409) before factor X2 suggested that the concentration of the surfactant had a beneficial influence on particle size. For NLC preparation, Tween 20 and Poloxamer 188 were used as the surfactants and co-surfactants, respectively. A critical factor in determining particle size is the amount of surfactant used in the recipe^{60,61}. At the optimal concentration, the surfactant molecules generate a thin film that covers the surface of the nanoparticles. This results in a reduction in PS and prevention of aggregation. However, suppose that the concentration of the surfactant increases above the optimum value. In this case, the molecules begin to collect on the surfaces of the nanoparticles, resulting in the excessive covering of the crystalline nanoparticles and an increase in their size⁶² (Eq. 6).

$$\text{Vesicle Size} = +330.29 + 5.73A + 29.56B - 26.56C - 43.75AB + 44.25AC + 33.75BC + 6.27A^2 + 48.52B^2 - 30.68C^2 \quad (6)$$

Parameters	PD aqueous solution	PD-NLCs
Intercept	1.368	1.939
Slope	-0.081	-0.027
C0 (mcg/mL)	23.349	86.876
k (h-1)	0.186	0.063
dose (mg)	10	10
dose (mcg)	1000	1000
vd (mL)	428.283	115.106
Vd (L)	0.007	0.115
t _{1/2} (h)	3.717	11.052
Clearance (L/h)	0.001	0.007
AUC _{0-t} (µg.h/mL)	5.962	21.844
AUC _{1-t} (µg.h/mL)	312.865	1002.6
AUC _{1-inf} (µg.h/mL)	5.310	340.828
AUC _{tot} (µg.h/mL)	324.138	1365.271
C _{max} (µg/mL)	1978.245	2851.346
T _{max} (h)	2.35	8.64
MRT (h)	6.983	21.398
Tf	----	15.94

Table 4. Pulmokinetic characteristics of a single dosage of PD-aqueous solution and PD-NLCs after instillation of PD into the intubated trachea.

When A, B, and C are model terms, the synergistic or antagonistic influence on the reaction is indicated by a positive or negative sign, respectively. A P-value of 0.05 indicates that all model parameters significantly affected the vesicle size. It is statistically likely that outcomes A2, B2, and C2 differ by chance.

An F-value of 39.06 indicates statistical significance. The likelihood of seeing such a large F-value due to noise is relatively low. In this case, it is essential to consider the model variables AB, C2, B2, and C2. An F-value of 1150.30 indicates that there is no goodness of fit. The 0.9475 Adjusted R² was quite close to the Predicted R². The primary responsibility for Adequate Precision is the evaluation of the signal-to-noise ratio. A minimum ratio of 4:1 was required. The data were sufficiently clear with an S/N ratio of 27,126. This concept may aid the navigation of the design world.

Effect of independent variables on Entrapment Efficiency

Entrapment efficiency (Eq. 7) was $42.5 \pm 5.3 - 81.4 \pm 7.1\%$, as shown in Table 2.

$$\begin{aligned} \text{Entrapment Efficiency} = & +60.51 - 0.7622A - 2.44B + 2.84C + 4.00AB - 6.50AC \\ & - 5.50BC + 0.2864A2 - 6.96B2 + 3.29C2 \end{aligned} \quad (7)$$

According to the literature, as shown by the second equation, an increase in the total lipid concentration increases EE, allowing for more room for the accommodation of drug particles. The addition of lipid also reduces the escape of the drug into the external phase^{30,63}. The amount of lipid liquid affects EE, with a rise in lipid leading to an increase in EE due to entrapment of the drug within the oil-enriched liquid. The initial effect of increasing the EE may be offset by the subsequent reduction in the EE caused by the trapping of the surfactant molecule inside the NLC⁶⁴. It has been shown that the time spent sonicating has a negligible effect on EE. As seen in the 3D plots of the particle size response, surface plots showing the effect of the independent variables on entrapment efficiency are shown in Fig. 4.

Negative and positive signs indicate synergistic and antagonistic effects on the responses of model variables A, B, and C, respectively. The model had a statistically significant F-statistic of 38.96. Noise is highly unlikely to contribute to such large F-values. In this case, it is essential to consider the model variables AB, C2, B2, and C2. For this model, a P value greater than 0.1000 is considered statistically insignificant. With an F-value of 34.03, a statistically significant discrepancy was observed between the two variables. A huge Lack of Fit F-value might have been caused by noise, although the likelihood was just 0.7%. In this case, the actual R² of 0.9473 was only 0.2% lower than the predicted R² of 0.7839. The primary function of adequate Precision is to calculate the signal-to-noise ratio. A minimum ratio of 4:1 was required. The signal-to-noise ratio was required to be greater than 26.197.

Effect of independent variables on PDI

The particle size distribution of nanoparticles can be measured using a metric called the particle size heterogeneity index (PDI). The PDI value may range from 0 (very monodisperse size distribution) to 1 (extremely polydisperse size distribution)⁶⁵. Regarding lipid nanoparticles, values under 0.3 are deemed acceptable and show a homogeneous size distribution, whereas values over 0.5 are polydisperse⁶⁶. A uniform distribution and a low PDI value best ensure particle stability and prevent aggregate formation. Variable PDI values were between

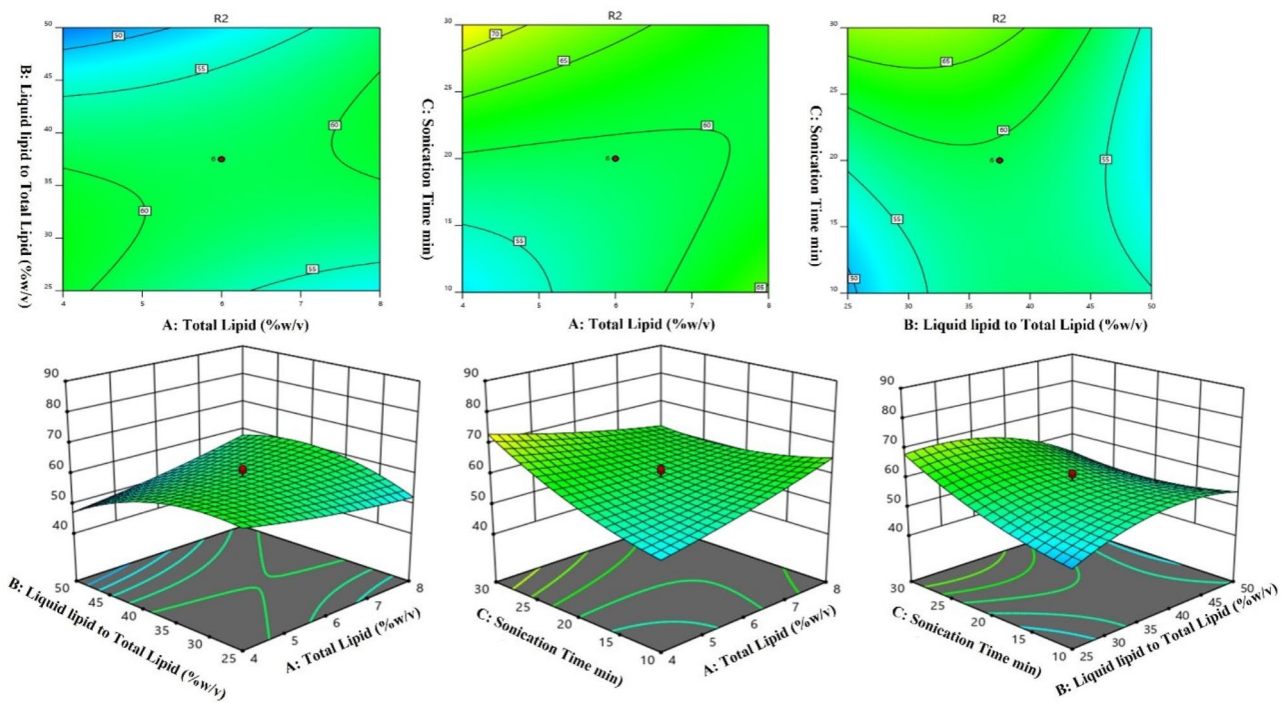


Fig. 4. counter and 3D response surface plots showing the effect of independent variables on Entrapment Efficiency,

0.13 ± 0.03 and 0.43 ± 0.13 . The surfactant had the greatest effect on the PDI value. An increase in the particle size distribution index (PDI) suggests that the preparation contains varying-sized particles. One possible explanation is that too many surfactant molecules were coated on the surface of the nanoparticles. Particles may increase if an excessive amount of Tween 20 causes the creation of a double layer⁶⁷. A decrease in particle size due to the formation of self-micelles at greater concentrations of free Poloxamer 188 molecules also contributed to the increase in PDI⁶⁸.

Effect of independent variables on Zeta Potential

The nanoparticles were negatively charged, as measured by the zeta potential, ranging from -32.5 ± 0.64 – 11.6 ± 0.26 mV. This parameter quantifies the electrostatic repulsion and attraction between nanoparticles, as represented by the surface charge. When the ZP was greater than 30 mV, the nanoparticles were stabilized, and their aggregation was prevented during storage⁶⁹. Significant ($p < 0.0001$) negative values preceding factor X2 (-1.681) and factor X1 \times 2 (-1), showing synergistic effects increasing negative ZP, indicating synergistic effects. A primary factor in the development of NLCs is the choice of surfactant. In this case, an anionic charge was imparted to the nanoparticle exteriors using Tween 20 and Poloxamer 188 as surfactants to stabilize the formulation. It has been hypothesized^{70,71} that the negatively charged phospholipids in the poloxamer are responsible for this charge. In addition, polarized poloxamer molecules may adsorb charge in water, creating an electric double layer analogous to an ionic layer between the particles and water⁷².

Optimization of PDLoaded NLC

To obtain the optimal formulation of PD-loaded NLCs, we used the Design-Expert desirability^{*} function to perform numerical optimization. When attempting to forecast an optimal value for each independent variable, numerical optimization relies on a single measure that combines all answers (Table 3). Our primary objective was to increase trapping efficiency while decreasing particle size. The ZP response was calibrated to be within the allowable range (less than 30 mV). We also attempted to reduce the amount of surfactant and increase that of the lipid phase. The software used for the experiment determined that a solution containing 6% total lipids, 0.5% surfactant combination, and 30 min of sonication would provide the best results (Fig. 5). Regarding entrapment efficiency, the model projected a value of 79.630%. In contrast, the model predicted a particle size of 172.464 nm. The desirability value is 0.960. The model was accurate when calculating and double-checking the optimum formula for all the three possible outcomes. Data showed that particle size was 159.8 ± 3.46 nm and entrapment effectiveness was 81.4 ± 7.1 . The model was verified and can adequately anticipate the optimum formulation results because these outcomes fall within the software's prediction ranges.

PS, PDI, and ZP

Vesicle size was greatly affected by the amount of lipid, and even a slight increase in quantity considerably increased its size. The vesicles in the liquid lipid solution shrank as their concentration increased. Tiny vesicles may help transfer drugs through the skin. Based on the results of the PDI 0.5 test, the formulation had a very

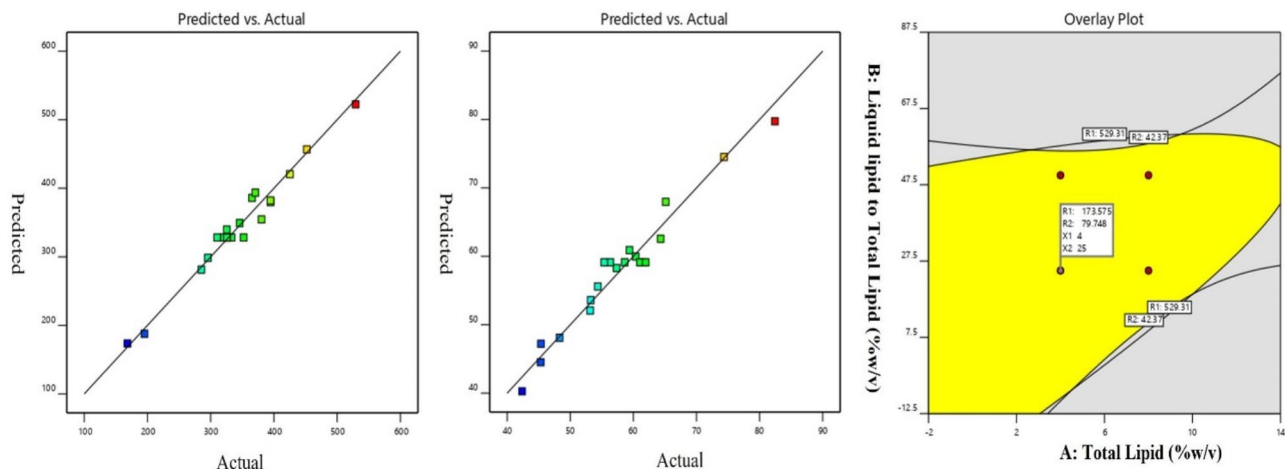


Fig. 5. The actual and predicted value of (A) particle size as Y1, (B) encapsulation efficiency as Y2, and (C) Overlay plot of dependent variables.

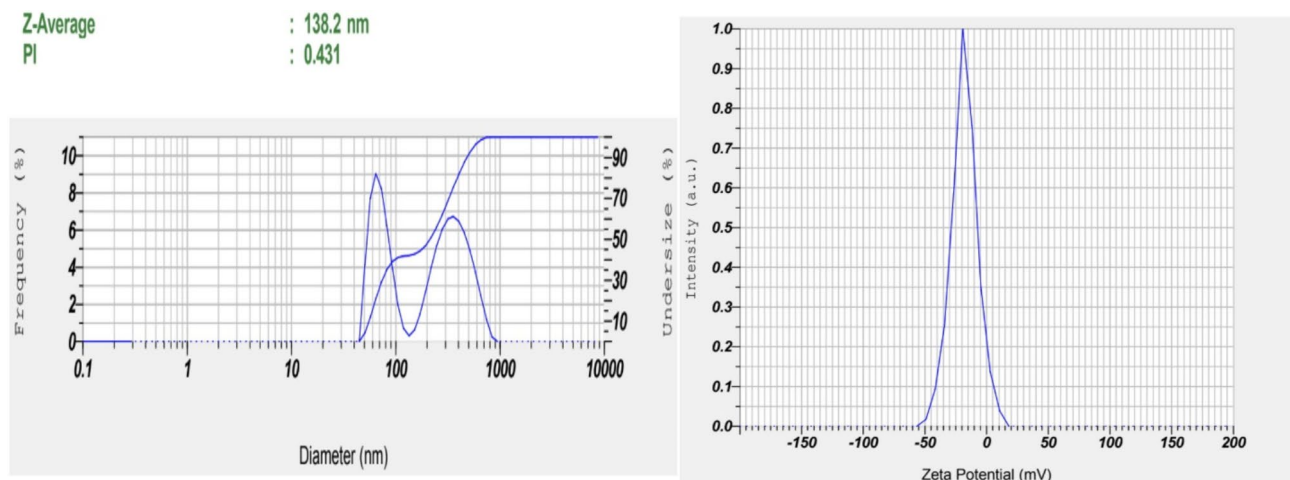


Fig. 6. (A) Particle size and (B) zeta potential of the improved PD-NLCs (F5).

narrow size distribution window. Most importantly, NLCs have diameters between 10 and 1000 nm. Vesicles with diameters of 300 nm or larger may transport drugs for a lengthy period, whereas smaller particles can release the drug quickly. Figure 6 shows the PS and ZP of the improved formulation. PD-NLCs had an average diameter of 159.8 ± 3.46 nm (PDI 0.13 ± 0.03 to 0.42 ± 0.61). Nanoparticles can be reduced in size to provide a more transparent solution for oral liquid formulations. Smaller particles and lower PDI might also help keep the solution suspended. The stability of the solution may be determined using the ZP of the colloidal solution. PD-NLCs had a high ZP of (-32.5–0.64 mV), indicating that they were highly stable (Fig. 6). Particles may be less likely to clump together, because they are more likely to oppose each other. Particle dispersion was more uniform when the PDI value was low. Measurement of the ZP indicates the stability of the nanoformulations. A smaller particle size (103 to 127 nm) for NLCs preparation was investigated by Fardin et al.⁷³.

Drug entrapment (EE) and drug loading (DL)

NLCs had an entrapment effectiveness of $81.4 \pm 7.1\%$ w/v, according to the study. In contrast to hydrophilic drugs, lipophilic drugs have an inherent ability to solubilize lipids more readily. As a result, the lipophilic properties of lipids render them more entrapped. According to our calculations, the % DL was $15.62 \pm 0.9\%$ w/v. Researchers led by Elmowafy investigated the use of DL-NLCs to circumvent oral delivery problem⁷⁴. According to their research, They determined that encapsulation effectiveness ranges from 76.2 to 122.4%. The high % of liquid lipid matrix (Capryol® PGMC) produces significant crystalline order flaws, which leads to a better room for the drug molecules to entrap and enhance the % EE.

For drug content and release experiments, the calibration curve of the HPLC method ($r^2 = 0.998$) was linear at concentrations of 0.05–2 g/mL. With a 20 ng/mL detection limit, the precision was less than 10% inter-and intraday. The entrapment efficiency of NLCs is closely related to the drug-to-lipid weight ratio, as shown in Fig. 4.

They increased the weight ratio of drug to lipid from 4 to 8%, followed by excellent drug entrapment to reduce the amount of lipids in lipids. Loaded and entrapment efficiencies were affected by oleic acid concentration. Increasing the oleic acid content can enhance drug entrapment efficiency. Liquid lipids incorporated into solid lipids have been shown in previous investigations to cause significant disruptions in the crystal arrangement. The DL capacity and EE increased owing to the massive crystal lattice defects that emerged from this process. Other factors had little effect on the drug content, as shown in Fig. 4.

Production yield

All 20 batches had a production yields ranging from 38 to 52%. The optimized batch production yield was 48.65%. The poor production yield during homogenization is caused by dispersion adhering to the glass container or material loss during collection.

Morphological characterization

PD-NLCs were studied using scanning electron microscopy (SEM) to examine their surface morphology (SEM). Particles with smooth surfaces are visible in the photograph (Fig. 7A). There was no evidence of particle aggregation in this study. There was no change in particle size. Tissue-optimized electron microscopy images (Fig. 7B) show the formulation of the PD-NLCs. The resulting NLCs formulation had a smooth, monodisperse, and spherical shape with defined boundaries between each particle. The TEM-measured particle diameters were in agreement with the DLS-measured particle diameters. In accordance with the photon correlation spectroscopy findings, the AFM images of the nanoparticles (Fig. 7C) showed a spherical and round form 150–200 nm in diameter.

However, dynamic light scattering measurements showed that the particle sizes reported by TEM and AFM were smaller than previously thought. It is possible that these discrepancies were revealed using different methods for estimating body mass. According to DLS measurements, the hydrodynamic size of a particle consistently exceeds that established using TEM and AFM.

Solid state characterizations

FTIR spectroscopy

FTIR was performed to study the possible interactions between the excipients and medicines. The physical mixture and formulation, appearance/loss of peaks, and broadening and sharpening of peaks were observed in the physical mixture and formulation. It was used to determine if the drug, polymer, and formulation were all compatible with each other (Fig. 8). The 3045, 2933, and 1599 cm^{-1} C=O, C-H, and aromatic C=C stretching vibration peaks found for a pure substance (PD) supported the identification of the drug. The most conspicuous infrared peak of the physical mixture was PD. The molecular structure of the drug was not altered when mixed with the lipids. A single peak was produced by combining several frequencies of the PD-NLCs IR spectra, which showed constructive inference. The FTIR spectra of the pure drug, the physical combination, and the final formulation are shown in Fig. 8a. According to these results, the drug was not exposed to the stress of the process parameters that would have caused degradation. In contrast, drugs and excipients showed no chemical interactions.

DSC

The physical characteristics of the pure drug, stearic acid, oleic acid, and PD-NLCs were examined by DSC (Fig. 8B). Stearic acid and the physical combination (drug + stearic acid + oleic acid + Tween 20) did not have a distinct endothermic peak, indicating the amorphous structure of the polymer. The sharp endotherm confirms the crystalline nature of the drug at 110.9 °C, which correlates with the melting point. An endothermic peak at 110.9 °C in the DSC thermogram of PD-loaded formulation has been verified to be molecularly distributed in the polymeric matrix.

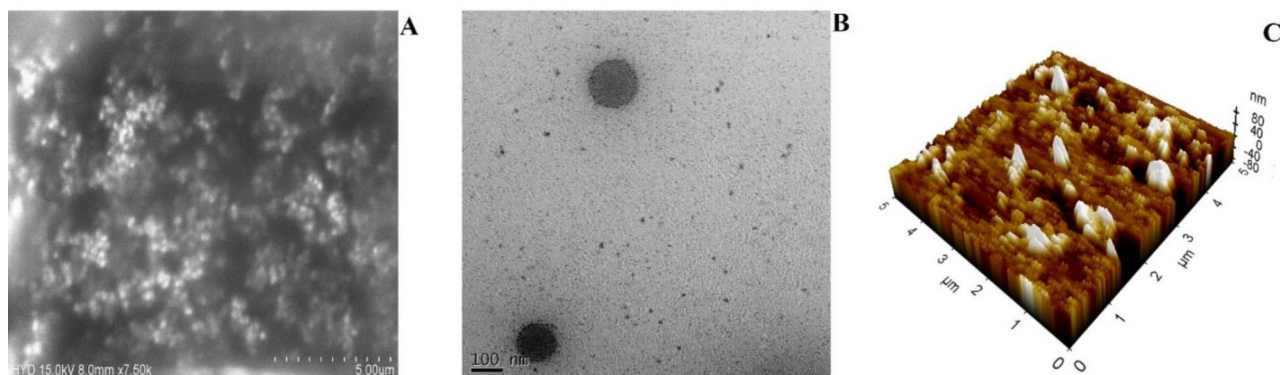


Fig. 7. Morphological characterization of Optimized NLCs (F5) (A) SEM, (B) TEM, and (C) AFM.

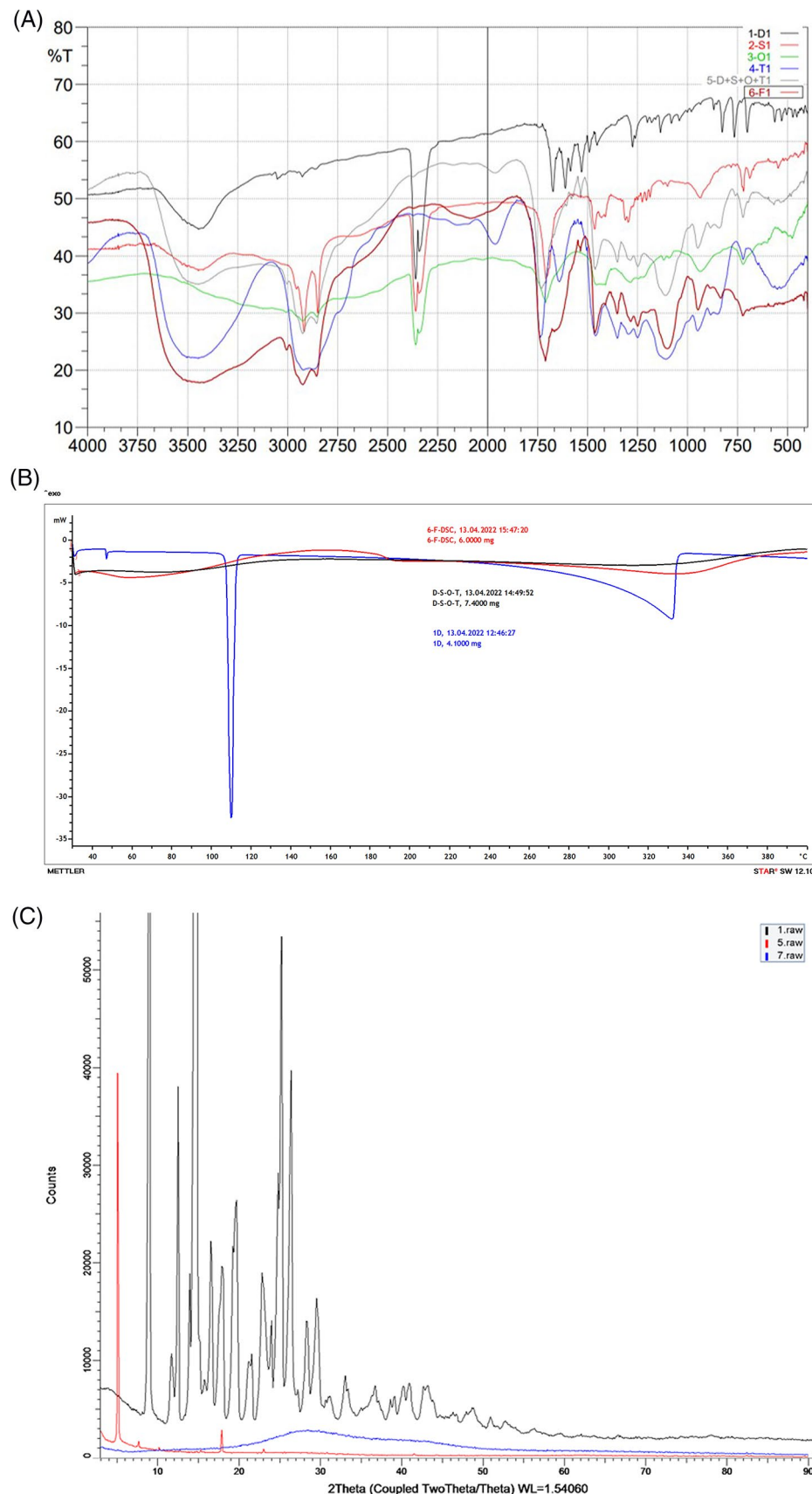


Fig. 8. (A) FTIR spectroscopy of (1) Drug, (2) Stearic acid, (3) Oleic acid, (4) Tween 20, (5) Physical Mixture, and (6) Formulation. (B) DSC thermographs of (1) Drug, (2) Physical Mixture, and (3) Optimized NLCs formulation (F5). (C) Powdered X-Ray diffractogram of 1. Drug, 5. Physical Mixture, and 7. Optimized NLCs formulation (F5)

XRD study

To ensure that the crystalline character of PD was significantly diminished in the final formulation, XRD was performed using DSC. Figure 8C displays XRD data for various polymers, a solid lipid, a liquid lipid, Tween 20, the physical combination, and the optimized formulation. The diffraction patterns of the formulations (10.329°, 14.816°, 18.867°, and 23.735°), the drug (14.769° and 15.728°), and the lipids (5.593°, 19.686°, 22.618°, and 23.694°) all had several diffraction peaks. The generated NLCs did not exhibit the expected XRD pattern and lacked the critical peaks that indicated the presence of these substances. The results suggest a recrystallization process that led to the formation of less organized crystals. The PD firm peaks indicate the drug's crystalline nature of the drug at 13.873°, 17.457°, 19.941°, 20.826°, and 21.688°. The absence of these peaks in the NLCs suggested an amorphous form of the drug. Several peaks in the XRD patterns of the physical mixtures were preserved from the lipids and surfactant. The XRD results matched the DSC results.

In-vitro drug release studies

A 24-hour in vitro release study utilized a dialysis bag in modified simulated lung fluid (mSLF; pH 7.4). The time-dependent release of the drug from the aqueous PD solution and PD-NLCs is shown in Fig. 9. PD aqueous solution and PD-NLCs released approximately 100% and 21.12% of the formulation, respectively, after 2.5 h. PD-NLCs took more than 24 h to remove 100% of the drug, showing a sustained drug release following lipids' encapsulation. To further understand the mechanism of PD-NLC drug release, we fitted several kinetic models to the release data. An R^2 of 0.987 was the best match for the release from PD-NLCs in the Higuchi matrix model. Korsmeyer–model Peppa's produced an R^2 of 0.880 with n (the release mechanism) set at 0.829 when data on release were fitted. We hypothesized a non-Fickian diffusion-controlled release of PD.

Cell viability

To determine the optimal dilution for the permeability tests, the MTS assay was first used to compare the cytotoxicity of the loaded and unloaded NLCs. Cell viability was not substantially decreased at dilutions of 1:150 for both NLCs and PD-NLCs compared with untreated cells. Exposure for 3 h resulted in a 5% decrease in cell viability (Fig. 10). Consequently, the dilution ratio for the permeability studies was set to 1:150. Because oral formulations are diluted between 1:200 and 1:1000 with biological fluids after oral delivery^{24,25}, this number may also reflect in vivo circumstances.

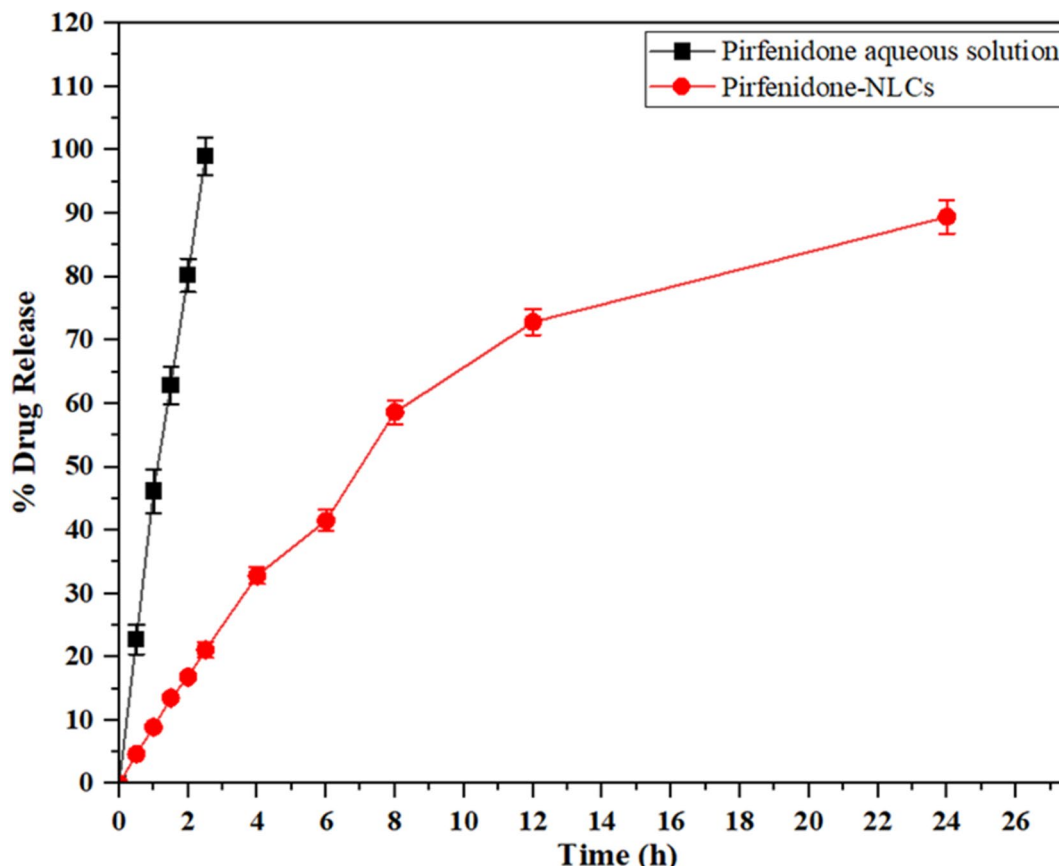


Fig. 9. PD release from PD-aqueous solution and PD-NLCs in vitro. The data averages three repetitions, with the error bar indicating the standard deviation.

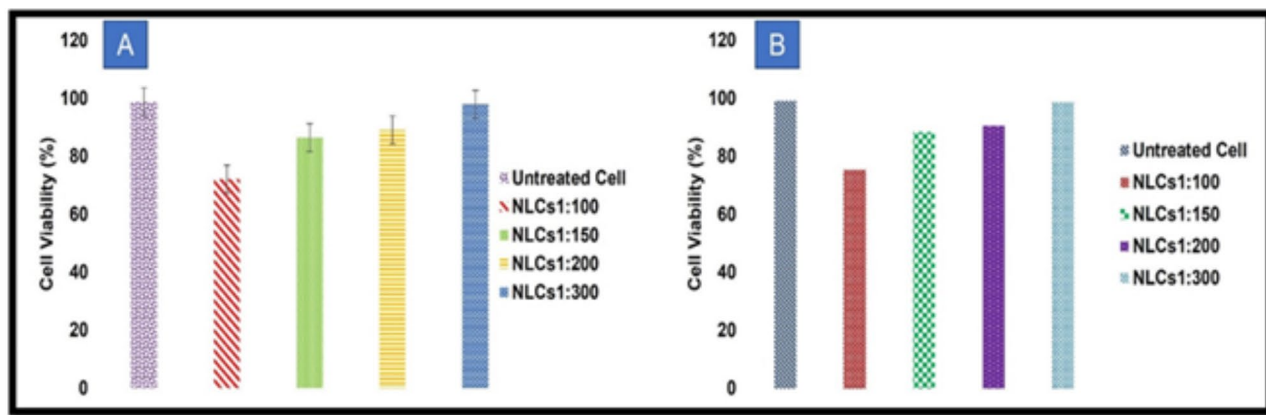


Fig. 10. Cytotoxicity on Caco-2 cell line (% vs. untreated cells) of (a) NLCs and (b) PD-NLCs at different dilutions (1:100, 1:150, 1:200, and 1:300) after 3 h of exposure. Data are shown as mean \pm standard error ($n=3$). * = $p < 0.05$.

Permeability study on Caco-2 cells

The Caco-2 cell line is a benchmark for assessing paracellular permeability, active efflux across the intestinal epithelium, paracellular diffusion, and active transport processes. Caco-2 cells exhibit substantial mucin content. Caco-2 cells serve as an effective model for predicting the effect of the mucus layer of the intestinal epithelium on penetration. The permeability of PD was assessed using passive diffusion after two hours of incubation in G1F and two hours in SIF using unformulated PD (PBS solution). This generated PD (PD-NLCs) at an equivalent concentration. After 2 h of incubation with Caco-2 cells, the apparent permeability (Papp) of the PD solution was $1.23 \pm 0.06 \times 10^{-8}$ cm/s, while that of PD-NLCs was $(5.21 \pm 1.26) \times 10^{-6}$ cm/s. Surfactants in the formulation may account for this enhancement. Lipids impede P-gp activity, whereas ethanol enhances penetration and solubilizes poorly water-soluble active compounds. This study demonstrated that LN's markedly enhanced PD permeability through the Caco-2 cell monolayer and mucus layer produced by the cells, indicating that this method may augment therapeutic efficacy. The literature indicates that PEG coating or PEGylation strategies enhance nanoparticle diffusion within the mucus layer. Two PEGylated surfactants, Tween 20 and Poloxamer 188, were used in the formulation of the PD-NLCs. These surfactants may enhance the mucus-penetrating properties of the formulated nanoparticles, thereby facilitating drug administration to the gastrointestinal tract and mucosal surface.

In vitro cytotoxicity study

Low toxicity is necessary for PD-NLC formulations to be appropriate for human use (Fig. 11). Thus, nanoparticles were evaluated in human lung cell lines in vitro to ensure their safety. For the MTT assay, the mitochondrial enzyme succinate dehydrogenase cleaves MTT, a yellow tetrazolium salt, into crystals of dark blue formazan that are insoluble in water. At various doses, the cytotoxicity of PD-NLCs was compared to that of the PD-aqueous solution in A549 cells. Cytotoxicity studies showed that cell viability decreased as the drug concentration increased. The R^2 value of the plot of %viability of cells versus drug concentration ($\mu\text{mol/L}$) was used to obtain the IC_{50} value. PD was found to have an IC_{50} value of $72.13 \pm 3.29 \mu\text{mol/L}$, whereas PD-NLCs had an IC_{50} value of $110.29 \pm 2.19 \mu\text{mol/L}$. After 24 h of exposure to the Placebo-NLCs formulation, cell viability reached $95.37 \pm 3.52\%$. Nonessential fatty acid (NLC) components are less harmful to cells. The creation of NLCs means that drugs may be delivered to the respiratory system. Researchers suggest that the biocompatibility of the excipients used in the NLC formulation is responsible for the lower toxicity of PD-NLCs compared to pure drugs. The lower toxicity of PD-NLCs is partly attributable to the drug's connection with the nanoparticles and prolonged release. Lipid glycerides are the primary constituents of NLCs formulations because they are biocompatible and well-tolerated by living organisms. As a result, the research found that PD-NLCs may be safely administered through the pulmonary route.

In vivo pulmokinetic

Using a cascade impactor in vitro, it was discovered that the primary and secondary bronchi and terminal lung bronchi of the trachea had increased deposition at stages 3, 4, and 5⁴⁶. PD NLCs may accumulate in the lower lobes of lungs when administered intravenously. Figure 12 shows the time-dependent concentrations of -in LH and BAL, whereas Table 4 lists the resulting kinetic parameters. This study demonstrated that the pharmacokinetics and release properties of the encapsulated PD were altered. The PD-aqueous solution and PD-NLCs were injected into the trachea, and PD-aqueous solution and PD-NLCs were recovered from the BAL. There was 38.26 ± 2.34 and $76.57 \pm 1.35\%$ PD recovery in the first h for PD-aqueous solution and PD-NLCs. Using PD-aqueous solution and PD-NLCs, the concentration of PD in BAL was reduced to 3.98 ± 0.25 and $4.68 \pm 0.22\%$ after 4 and 12 h, respectively. PD was not detected in the BAL 4 h after intra-tracheal PD-aqueous solution infusion. After 12 h, no drug was found in the BAL of rats administered the PD-NLCs. Drug levels in the lung tissue decreased after 8 h, indicating that the drug had been removed.

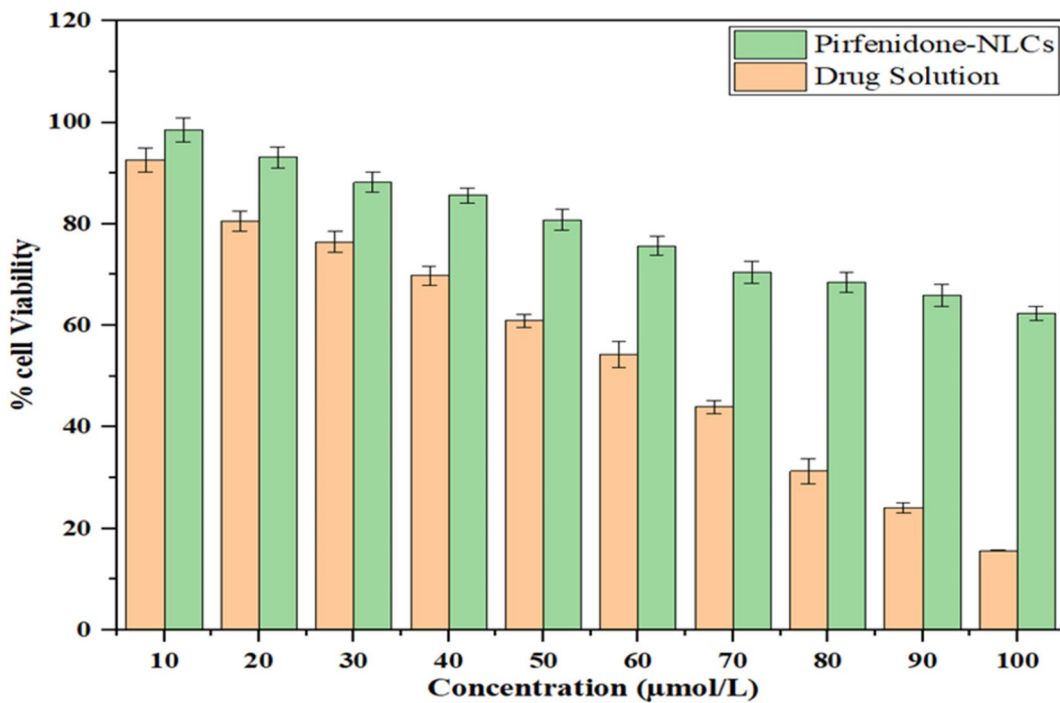


Fig. 11. In vitro viability of PD-NLCs and PD in A549 cells. The MTT assay examines the cytotoxicity of PD-aqueous solution and PD-NLCs at various cell doses.

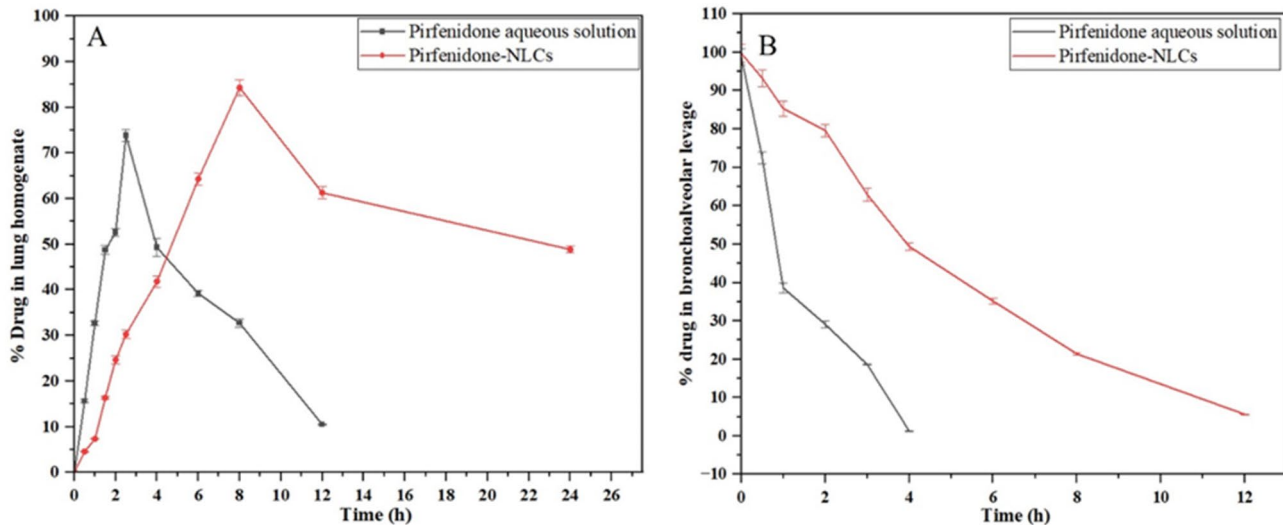


Fig. 12. (A) Aqueous PD solution and PD-NLCs were intratracheally injected into Wistar rats for 24 h, and PD concentrations in lung homogenate were determined (LH). (B) PD concentration in BAL. Mean Standard Deviation (SD) for $n=6$ data points.

At the beginning of the trial, the PD solution had a greater drug concentration in the lung tissue (up to 2 h). The PD aqueous solution had a higher concentration of PD, which was readily accessible for absorption. When the PD solution was administered to rats, the C_{max} was reported to be $1978.2456 \pm 175 \mu\text{g/g}$ of lung tissue after two hrs (T_{max}). Compared to PD aqueous solution, intra-tracheal delivery of PD-NLCs resulted in much higher C_{max} ($2851.3459 \pm 112.35 \mu\text{g per gm}$ of lung tissue) and T_{max} of 4 h. When administered with PD aqueous solution, PD cleared the lungs quickly, and the PD levels in the lung tissue were negligible after 24 h.

Alternatively, PD-NLC's gradual and sustained outflow of the PD-NLCs delayed T_{max} . In addition, the shelf life of the drug was extended using the PD-NLCs as a formulation. According to the AUC value, the bioavailability of PD-NLCs was approximately 12-times more than that of the PD-aqueous solution. Better peripheral deposition and mucociliary migration may result in higher and more persistent drug concentrations

Incubation time	Size (nm)	PDI	% recovery
0	159.8 ± 3.46	0.13 ± 0.03	98.25
2SGF	164.3 ± 5.34	0.18 ± 0.21	96.34
2SGF + 2SIF	178.9 ± 6.51	0.26 ± 0.05	82.67
2SGF + 4SIF	164.2 ± 8.37	0.22 ± 0.12	75.38

Table 5. Physical and chemical stability of PD-NLCs.

Time	%EE		Size (nm)		PDI		Zetapotential (mV)	
	5 ± 2 °C	25 °C ± 2 °C	5 ± 2 °C	25 °C ± 2 °C	5 ± 2 °C	25 °C ± 2 °C	5 ± 2 °C	25 °C ± 2 °C
0	81.4 ± 7.1	81.4 ± 7.1	159.8 ± 3.46	159.8 ± 3.46	0.13 ± 0.03	0.13 ± 0.03	-32.5 ± 0.64	-32.5 ± 0.64
1	80.3 ± 1.05	80.9 ± 2.41	168.3 ± 5.64	165.3 ± 6.23	0.15 ± 0.02	0.14 ± 0.06	-30.2 ± 0.12	-29.6 ± 0.05
3	77.9 ± 0.09	78.6 ± 0.94	172.1 ± 2.91	16,938 ± 8.15	0.17 ± 0.04	0.15 ± 0.04	-28.4 ± 0.31	-27.1 ± 0.09
6	72.5 ± 1.35	76.1 ± 1.65	190.3 ± 3.46	178.4 ± 4.29	0.19 ± 0.01	0.16 ± 0.02	-26.1 ± 0.26	-25.8 ± 0.01

Table 6. Stability statistics of dispersion-loaded NLCs PD at 4 and 25 °C.

at the target site. Incorporating drugs into nanoparticles, particularly those smaller than 500 nm, increases lung deposition and decreases mucus removal by surface energy.

In contrast to the micronized drug, nano-salbutamol was found to interact more strongly with the lung membrane⁷⁵. Nanoparticles containing a drug may have a more remarkable ability to interact with the lung membrane, increasing the pharmacokinetic characteristics of the drug and hence its therapeutic index. The continuous release of the drug by PD-NLCs may have contributed to the longer $t_{1/2}$ and mean residence time (MRT) resulting from reduced elimination rates. For the PD-aqueous solution, $t_{1/2}$ and MRT increased by approximately 3.101-fold after intratracheal injection of the PD-NLCs. In addition, because of their small size and lipophilic nature, NLCs have mucoadhesive properties that might lengthen the duration of the drug in the lungs.

PD-NLCs have a 15.94 targeting factor, which indicates that PD-NLCs have more significant targeting potential. The particle size and composition of the formulation were responsible for the high level of lung PD-NLC deposition. For a long period of time, macrophages cannot remove particles smaller than 260 nm. Stearic acid and oleic acid are responsible for the adsorption of drug-loaded NLCs on the airway epithelium, inhibiting mucociliary lung passage.

Stability of PD-NLCs in gastric and intestinal simulated fluids

The size, PDI, and R% of PD were measured after various incubation durations to assess the stability of the PD-NLCs in SGF and SIF. There was a 150-fold dilution of PD-NLCs in SGF and a 10-fold dilution in SGF, followed by a 15-fold dilution in SIF. A total dilution of 1:150 was chosen for more reliable results, as this concentration was also used in the permeability testing of Caco-2 cells. Due to the decreased water concentration in the stomach compared to that in the intestinal tract, a minor dilution of SGF was used.

The hydrolysis of surfactants often leads to aggregation, whereas fast enzymatic degradation may result in size reduction. After 2 h of incubation in SGF, there was no change in the size or PDI. After 2 h of incubation with SIF, a marginal increase in size was observed. Significant growth was observed after 4 h of incubation (Table 5). After 4 h in SIF, the PDI did not significantly improve. *The samples* were visually inspected, and their sizes and PDIs were measured to detect any deterioration caused by the acidity of the gastric media or the action of digestive enzymes (pepsin, pancreatin, and lipase) throughout the experiment. In addition, the size increase of approximately 37 nm cannot be related to nanoparticle gathering, ruling out the possibility of aggregation events. This is because sample homogeneity was preserved despite the increase in the average nanoparticle diameter.

Consequently, PD-NLCs are chemically and physically stable in SGF and SIF. The surfactant properties significantly influence the stability of the nanoparticles. Tween 20 is resistant to lipase digestion because it does not possess a typical triglyceride structure. Stearic acid has a pKa of approximately 4.75, indicating that it is stable under acidic conditions in the stomach. In addition, oleic acid is derived from stearic acid by covalent grafting using PEG 1000 chains, which creates a hydrophilic steric barrier around the NLCs and boosts their stability. Interaction with lipases is impeded to a greater extent as the length of the ethylene oxide chains increases. Surfactants act as a physical barrier, slowing down or speeding up the degradation rate as needed and stabilizing the nanoparticles to prevent flocculation and coalescence.

Storage stability of prepared dispersion

The dispersion of PD-NLC that had been synthesized was stable for six months when stored. There was little shift in dimensions, such as size, PDI, ZP, or % EE. Table 6 shows the dispersion stability statistics for the PD-NLCs. Consequently, the PD-NLC dispersion exhibited limited or no drug ejection during storage, as evidenced by the study findings. As shown by the particle size and PDI, the dispersion of NLCs with no nanocarrier aggregation was stable. This indicates that the dispersion of PD-NLCs was acceptable from a regulatory perspective, which places a premium on formulation stability.

Conclusions

NLCs have raised the bar for solubility and bioavailability in cosmetics, pharmaceuticals, and food industries. The optimized PD-loaded NLCs, a homogenization process with various lipids and surfactants, was used in this study. Physical stability, high EE, small vesicle size, and long-term drug release were observed in NLCs made with various amounts of solid and liquid lipids (F5). Owing to their slow and sustained release profiles, NLCs can maintain stable drug concentrations in the skin. It has been shown that topical application of water-soluble drug in NLCs leads to more significant skin drug accumulation. The PD was effectively encapsulated using Stearic acid and oleic acid. This procedure resulted in particle sizes of 159.8 nm and an EE ratio of $81.4 \pm 7.1\%$. PD-loaded NLCs in the buffer provided controlled and sustained release of the drug (pH 7.4). PD-loaded NLCs were non-toxic and compatible with lung cell lines in an in vitro cytotoxicity study. This might have led to a more significant concentration of the drug in the lower portion of the rat lung. PD-loaded NLCs were shown to enhance lung deposition in an in vivo intratracheal instillation investigation. According to research findings, the PD-loaded NLCs formulation might be used to strengthen pharmacokinetic characteristics and establish the possibility of pulmonary targeting. According to this study, PD can be delivered to the lungs via NLCs.

Data availability

All data generated or analyzed during this study are included in this published article.

Received: 19 December 2024; Accepted: 17 February 2025

Published online: 03 April 2025

References

1. Takeda, Y., Tsujino, K., Kijima, T. & Kumanogoh, A. Efficacy and safety of pirfenidone for idiopathic pulmonary fibrosis. *Patient Prefer Adherence*. **8**, 361 (2014).
2. Hilberg, O., Simonsen, U., du Bois, R. & Bendstrup, E. Pirfenidone: Significant treatment effects in idiopathic pulmonary fibrosis. *Clin. Respir. J.* **6**, 131–143 (2012).
3. Richeldi, L., Yasothan, U., Kirkpatrick, P. & Pirfenidone *Nat. Rev. Drug Discov.* **10**, 489–491 (2011).
4. Taniguchi, H. et al. Pirfenidone in idiopathic pulmonary fibrosis. *Eur. Respir. J.* **35**, 821–829 (2010).
5. Carter, N. *J. Pirfenidone Drugs* **71**, 1721–1732 (2011).
6. Seto, Y., Inoue, R., Kato, M., Yamada, S. & Onoue, S. Photosafety assessments on pirfenidone: Photochemical, photobiological, and pharmacokinetic characterization. *J. Photochem. Photobiol. B Biol.* **120**, 44–51 (2013).
7. Müller, R. H., Mäder, K. & Gohla, S. Solid lipid nanoparticles (SLN) for controlled drug delivery - A review of the state of the art. *Eur. J. Pharm. Biopharm.* **50**, 161–177 (2000).
8. Muller, H., Shegokar, R., Keck, M. & R. & 20 years of lipid nanoparticles (SLN & NLC): Present state of development & industrial applications. *Curr. Drug Discov Technol.* **8**, 207–227 (2011).
9. Beloqui, A., Solinís, M. Á., Rodríguez-Gascón, A., Almeida, A. J. & Préat, V. Nanostructured lipid carriers: Promising drug delivery systems for future clinics. *Nanomed. Nanotechnol. Biol. Med.* **12**, 143–161 (2016).
10. Beloqui, A., del Pozo-Rodríguez, A., Isla, A., Rodríguez-Gascón, A. & Solinís, M. Á. Nanostructured lipid carriers as oral delivery systems for poorly soluble drugs. *J. Drug Deliv. Sci. Technol.* **42**, 144–154 (2017).
11. Ganesan, P. & Narayanasamy, D. Lipid nanoparticles: Different preparation techniques, characterization, hurdles, and strategies for the production of solid lipid nanoparticles and nanostructured lipid carriers for oral drug delivery. *Sustain. Chem. Pharm.* **6**, 37–56 (2017).
12. Poonia, N., Kharb, R., Lather, V. & Pandita, D. Nanostructured lipid carriers: Versatile oral delivery vehicle. *Futur Sci. OA*. **2**, FSO135 (2016).
13. Lawless, E., Griffin, B. T., O'Mahony, A. & O'Driscoll, C. M. Exploring the impact of drug properties on the extent of intestinal lymphatic transport-in vitro and in vivo studies. *Pharm. Res.* **32**, 1817–1829 (2015).
14. Chaturvedi, S., Garg, A. & Verma, A. Nano lipid based carriers for lymphatic voyage of anti-cancer drugs: An insight into the in-vitro, ex-vivo, in-situ and in-vivo study models. *J. Drug Deliv. Sci. Technol.* **59**, 101899 (2020).
15. Pandya, P., Giram, P., Bhole, R. P., Chang, H. I. & Raut, S. Y. Nanocarriers based oral lymphatic drug targeting: Strategic bioavailability enhancement approaches. *J. Drug Deliv. Sci. Technol.* **64**, 102585 (2021).
16. Poovi, G. & Damodharan, N. Lipid nanoparticles: A challenging approach for oral delivery of BCS Class-II drugs. *Futur J. Pharm. Sci.* **4**, 191–205 (2018).
17. Zhu, Y. et al. Nanostructured lipid carriers as oral delivery systems for improving oral bioavailability of nintedanib by promoting intestinal absorption. *Int. J. Pharm.* **586**, 119569 (2020).
18. Rangaraj, N., Pailla, S. R., Shah, S., Prajapati, S. & Sampathi, S. QbD aided development of ibrutinib-loaded nanostructured lipid carriers aimed for lymphatic targeting: Evaluation using chylomicron flow blocking approach. *Drug Deliv. Transl. Res.* **10**, 1476–1494 (2020).
19. Shrivastava, S., Gidwani, B. & Kaur, C. D. Development of mebendazole loaded nanostructured lipid carriers for lymphatic targeting: Optimization, characterization, in-vitro and in-vivo evaluation. *Part. Sci. Technol.* **39**, 380–390 (2021).
20. Hao, J. et al. Development and optimization of solid lipid nanoparticle formulation for ophthalmic delivery of chloramphenicol using a Box-Behnken design. *Int. J. Nanomed.* **6**, 683 (2011).
21. Ravi, P. R., Aditya, N., Kathuria, H., Malekar, S. & Vats, R. Lipid nanoparticles for oral delivery of raloxifene: Optimization, stability, in vivo evaluation and uptake mechanism. *Eur. J. Pharm. Biopharm.* **87**, 114–124 (2014).
22. Ranch, K. M. et al. Optimization of a novel in situ gel for sustained ocular drug delivery using Box-Behnken design: In vitro, ex vivo, in vivo and human studies. *Int. J. Pharm.* **554**, 264–275 (2019).
23. Vanti, G. et al. The anti-arthritis efficacy of khellin loaded in ascorbyl decanoate nanovesicles after an intra-articular administration. *Pharmaceutics* **13**, 1275 (2021).
24. Risaliti, L. et al. Hydroxyethyl cellulose hydrogel for skin delivery of khellin loaded in ascosomes: Characterization, in vitro/in vivo performance and acute toxicity. *Int. J. Biol. Macromol.* **179**, 217–229 (2021).
25. Ben Hadj Ayed, O., Lassoued, M. A. & Sfar, S. Quality-by-design Approach Development, characterization, and in Vitro Release mechanism elucidation of nanostructured lipid carriers for Quetiapine Fumarate oral delivery. *J. Pharm. Innov.* **17**, 1–16 (2021).
26. Jazuli, I. et al. Optimization of nanostructured lipid carriers of lurasidone hydrochloride using Box-Behnken design for brain targeting: In vitro and in vivo studies. *J. Pharm. Sci.* **108**, 3082–3090 (2019).
27. Negi, L. M., Tariq, M. & Talegaonkar, S. Nano scale self-emulsifying oil based carrier system for improved oral bioavailability of camptothecin derivative by P-Glycoprotein modulation. *Colloids Surf. B Biointerfaces* **111**, 346–353 (2013).
28. Esposito, E., Drechsler, M., Cortesi, R. & Nastruzzi, C. Encapsulation of cannabinoid drugs in nanostructured lipid carriers. *Eur. J. Pharm. Biopharm.* **102**, 87–91 (2016).

29. Azevedo, M. A. et al. Rhamnolipids-based nanostructured lipid carriers: Effect of lipid phase on physicochemical properties and stability. *Food Chem.* **344**, 128670 (2021).
30. Alam, T. et al. Adaptation of quality by design-based development of isradipine nanostructured-lipid carrier and its evaluation for in vitro gut permeation and in vivo solubilization fate. *J. Pharm. Sci.* **107**, 2914–2926 (2018).
31. Pinto, F., de Barros, D. P. C., Reis, C. & Fonseca, L. P. Optimization of nanostructured lipid carriers loaded with retinoids by central composite design. *J. Mol. Liq.* **293**, 111468 (2019).
32. Wang, X. et al. Development of a nanostructured lipid carrier-based drug delivery strategy for apigenin: Experimental Design based on CCD-RSM and evaluation against NSCLC in Vitro. *Molecules* **28**, 6668 (2023).
33. Ye, Q. et al. Development and evaluation of puerarin-loaded controlled release nanostructured lipid carries by central composite design. *Drug Dev. Ind. Pharm.* **47**, 113–125 (2021).
34. Moolakkadath, T. et al. Development of transtethosomes formulation for dermal fisetin delivery: Box-behnken design, optimization, in vitro skin penetration, vesicles–skin interaction and dermatokinetic studies. *Artif. Cells Nanomed. Biotechnol.* **46**, 755–765 (2018).
35. Shadambikar, G. et al. Formulation development of itraconazole PEGylated nano-lipid carriers for pulmonary aspergillosis using hot-melt extrusion technology. *Int. J. Pharm. X.* **3**, 100074 (2021).
36. Saad, M., Garbuzenko, O. B. & Minko, T. Co-delivery of siRNA and an anticancer drug for treatment of multidrug-resistant cancer. *Nanomedicine* **3** (6), 761–776, (2008).
37. Singh, S. K. et al. Intranasal delivery of asenapine loaded nanostructured lipid carriers: Formulation, characterization, pharmacokinetic and behavioural assessment. *RSC Adv.* **6**, 2032–2045 (2016).
38. Pardeike, J., Hommoss, A. & Müller, R. H. Lipid nanoparticles (SLN, NLC) in cosmetic and pharmaceutical dermal products. *Int. J. Pharm.* **366**, 170–184 (2009).
39. Vanti, G., Bani, D., Salvatici, M. C., Bergonzi, M. C. & Bilia, A. R. Development and percutaneous permeation study of escinosomes, escin-based nanovesicles loaded with berberine chloride. *Pharmaceutics* **11**, 682 (2019).
40. Pardeike, J. et al. Development of an itraconazole-loaded nanostructured lipid carrier (NLC) formulation for pulmonary application. *Int. J. Pharm.* **419**, 329–338 (2011).
41. Pucek-Kaczmarek, A. Influence of process design on the preparation of solid lipid nanoparticles by an ultrasonic-nanoemulsification method. *Processes* **9**, 1265 (2021).
42. Üner, B., Özdemir, S., Taçs, Ç., Özsoy, Y. & Üner, M. Development of lipid nanoparticles for transdermal loteprednol etabonate delivery. *J. Microencapsul.* **39**, 1–27 (2022).
43. Liu, T. T., Liu, X. T., Chen, Q. X. & Shi, Y. Lipase inhibitors for obesity: A review. *Biomed. Pharmacother.* **128**, 110314 (2020).
44. Zaki, R. M., Ibrahim, M. A., Alshora, D. H. & El Ela, A. E. S. A. Formulation and evaluation of Transdermal Gel containing tacrolimus-loaded spanlastics: In vitro, ex vivo and in vivo studies. *Polym. (Basel.)* **14**, 1528 (2022).
45. Garg, N. K. et al. Quality by design (QbD)-enabled development of aceclofenac loaded-nano structured lipid carriers (NLCs): An improved dermatokinetic profile for inflammatory disorder(s). *Int. J. Pharm.* **517**, 413–431 (2017).
46. Piazzini, V. et al. Nanostructured lipid carriers as promising delivery systems for plant extracts: The case of silymarin. *Appl. Sci.* **8**, 1163 (2018).
47. Vanti, G. et al. Nanostructured lipid carriers can enhance oral absorption of khellin, a natural pleiotropic molecule. *Molecules* **26**, 7657 (2021).
48. Ministry of environment and forests, I. SOP _ Committee for the purpose of control and supervision of experiments on animals. Compend. CPCSEA. 1–144 (2010). (2018).
49. Kilkenny, C., Browne, W. J., Cuthill, I. C., Emerson, M. & Altman, D. G. Improving bioscience research reporting: The arrive guidelines for reporting animal research. *PLoS Biol.* **8**, 94–99 (2010).
50. Patil-Gadhe, A. & Pokharkar, V. Single step spray drying method to develop proliposomes for inhalation: A systematic study based on quality by design approach. *Pulm Pharmacol. Ther.* **27**, 197–207 (2014).
51. Philip, G. et al. A phase I randomized, placebo-controlled, dose-exploration study of single-dose inhaled montelukast in patients with chronic asthma. *J. Asthma.* **47**, 1078–1084 (2010).
52. Sarode, N., Chhabra, G. S., Luhar, S. & Jadhav, A. Development and validation of RP-HPLC method for the estimation of Montelukast sodium in bulk and in tablet dosage form. *Res. J. Sci. Technol.* **3**, 257–260 (2011).
53. Patel, N., Baldaniya, M., Raval, M. & Sheth, N. Formulation and development of in situ nasal gelling systems for quetiapine fumarate-loaded mucoadhesive microemulsion. *J. Pharm. Innov.* **10**, 357–373 (2015).
54. Moghaddam, S. M. M., Ahad, A., Aqil, M., Imam, S. S. & Sultana, Y. Optimization of nanostructured lipid carriers for topical delivery of nimesulide using box–behnken design approach. *Artif. Cells Nanomed. Biotechnol.* **45**, 617–624 (2017).
55. Tapeinos, C., Battaglini, M. & Ciofani, G. Advances in the design of solid lipid nanoparticles and nanostructured lipid carriers for targeting brain diseases. *J. Control Release* **264**, 306–332 (2017).
56. Li, T. S. C. Sea buckthorn: New crop opportunity. (1999).
57. Hejri, A., Khosravi, A., Gharanjig, K. & Hejazi, M. Optimisation of the formulation of \$β\$-carotene loaded nanostructured lipid carriers prepared by solvent diffusion method. *Food Chem.* **141**, 117–123 (2013).
58. Zhang, J., Fan, Y. & Smith, E. Experimental design for the optimization of lipid nanoparticles. *J. Pharm. Sci.* **98**, 1813–1819 (2009).
59. Vitorino, C., Carvalho, F. A., Almeida, A. J., Sousa, J. J. & Pais, A. A. C. C. The size of solid lipid nanoparticles: An interpretation from experimental design. *Colloids Surf. B Biointerfaces* **84**, 117–130 (2011).
60. Fathi, H. A., Allam, A., Elsabahy, M., Fetih, G. & El-Badry, M. Nanostructured lipid carriers for improved oral delivery and prolonged antihyperlipidemic effect of simvastatin. *Colloids Surf. B Biointerfaces* **162**, 236–245 (2018).
61. Gaba, B. et al. Nanostructured lipid (NLCs) carriers as a bioavailability enhancement tool for oral administration. *Drug Deliv.* **22**, 691–700 (2015).
62. Tan, S. W., Billa, N., Roberts, C. R. & Burley, J. C. Surfactant effects on the physical characteristics of amphotericin B-containing nanostructured lipid carriers. *Colloids Surf. Physicochem. Eng. Asp.* **372**, 73–79 (2010).
63. Subedi, R. K., Kang, K. W. & Choi, H. K. Preparation and characterization of solid lipid nanoparticles loaded with doxorubicin. *Eur. J. Pharm. Sci.* **37**, 508–513 (2009).
64. Javed, M. N., Kohli, K. & Amin, S. Risk assessment integrated QbD approach for development of optimized bicontinuous mucoadhesive limicubes for oral delivery of rosuvastatin. *AAPS PharmSciTech* **19**, 1377–1391 (2018).
65. Gaumet, M., Vargas, A., Gurny, R. & Delie, F. Nanoparticles for drug delivery: The need for precision in reporting particle size parameters. *Eur. J. Pharm. Biopharm.* **69**, 1–9 (2008).
66. Danaei, M. et al. Impact of particle size and polydispersity index on the clinical applications of lipidic nanocarrier systems. *Pharmaceutics* **10**, 57 (2018).
67. Chuacharoen, T. & Sabliov, C. M. Stability and controlled release of lutein loaded in zein nanoparticles with and without lecithin and pluronic F127 surfactants. *Colloids Surf. Physicochem. Eng. Asp.* **503**, 11–18 (2016).
68. Witayaudom, P. & Klinkesorn, U. Effect of surfactant concentration and solidification temperature on the characteristics and stability of nanostructured lipid carrier (NLC) prepared from rambutan (*Nephelium lappaceum* L.) kernel fat. *J. Colloid Interface Sci.* **505**, 1082–1092 (2017).
69. Freitas, C. & Müller, R. H. Effect of light and temperature on Zeta potential and physical stability in solid lipid nanoparticle (SLN™) dispersions. *Int. J. Pharm.* **168**, 221–229 (1998).
70. Rydhag, L. & Wilton, I. The function of phospholipids of soybean lecithin in emulsions. *J. Am. Oil Chem. Soc.* **58**, 830–837 (1981).

71. Wang, G. & Wang, T. Oxidative stability of egg and soy lecithin as affected by transition metal ions and pH in emulsion. *J. Agric. Food Chem.* **56**, 11424–11431 (2008).
72. Han, F., Li, S., Yin, R., Liu, H. & Xu, L. Effect of surfactants on the formation and characterization of a new type of colloidal drug delivery system: Nanostructured lipid carriers. *Colloids Surf. Physicochem. Eng. Asp.* **315**, 210–216 (2008).
73. Tamjidi, F., Shahedi, M., Varshosaz, J. & Nasirpour, A. Nanostructured lipid carriers (NLC): A potential delivery system for bioactive food molecules. *Innov. Food Sci. Emerg. Technol.* **19**, 29–43 (2013).
74. Elmowafy, M. & Al-Sanea, M. M. Nanostructured lipid carriers (NLCs) as drug delivery platform: Advances in formulation and delivery strategies. *Saudi Pharm. J.* **29**, 999–1012 (2021).
75. Ahmad, F. J. et al. Nano-Salbutamol dry powder inhalation: A new approach for treating broncho-constrictive conditions. *Eur. J. Pharm. Biopharm.* **71**, 282–291 (2009).

Acknowledgements

The Authors are thankful to Anurag University for their support in conducting this study.

Author contributions

Initiation, UH, PU, AC, MG, and PS; conceptualization; methodology; software; software validation; RJ, AK, AO and PS; formal analysis; investigation; PU, UH; resources; data curation; writing; preparation of the original draft; visualization; supervision; project administration; funding acquisition; AH, AK, AC and UH; writing, review, and editing: PA, AH, MG. The text has been reviewed and approved by all authors.

Funding

The authors extend their appreciation to the Deanship of Scientific Research at King Khalid University for funding this work through the Large Groups Project (Grant Number RGP.2/559/45).

Declarations

Ethics approval and consent to participate

The Institutional Animal Ethics Committee (IAEC) of Andhra University in Visakhapatnam (IAEC No: I/IAEC/AU/013/2021WR) approved our testing technique, which was developed under the CPCSEA guidelines. The in vivo procedure was performed according to the guidelines of the Committee for the Purpose of Control and Supervision of Experiments on Animals (CPCSEA). All in vivo studies complied with the ARRIVE criteria. This study was conducted in accordance with ARRIVE guidelines.

Consent for publication

Not applicable.

Competing interests

The authors declare no competing interests.

Additional information

Correspondence and requests for materials should be addressed to A.K.C. or M.G.

Reprints and permissions information is available at www.nature.com/reprints.

Publisher's note Springer Nature remains neutral with regard to jurisdictional claims in published maps and institutional affiliations.

Open Access This article is licensed under a Creative Commons Attribution-NonCommercial-NoDerivatives 4.0 International License, which permits any non-commercial use, sharing, distribution and reproduction in any medium or format, as long as you give appropriate credit to the original author(s) and the source, provide a link to the Creative Commons licence, and indicate if you modified the licensed material. You do not have permission under this licence to share adapted material derived from this article or parts of it. The images or other third party material in this article are included in the article's Creative Commons licence, unless indicated otherwise in a credit line to the material. If material is not included in the article's Creative Commons licence and your intended use is not permitted by statutory regulation or exceeds the permitted use, you will need to obtain permission directly from the copyright holder. To view a copy of this licence, visit <http://creativecommons.org/licenses/by-nc-nd/4.0/>.

© The Author(s) 2025